RIGA TECHNICAL UNIVERSITY

Dmitrijs Gorbačovs

FAILURE STUDY OF RUBBER-CORD FLEXIBLE COUPLINGS AND THEIR MOUNTING BOLTS

Summary of the Doctoral Thesis

RTU Press
Riga 2024

RIGA TECHNICAL UNIVERSITY
Faculty of Civil and Mechanical Engineering
Institute of Transport

Dmitrijs Gorbačovs
Doctoral Student of the Study Program "Transport"

FAILURE STUDY OF RUBBER-CORD FLEXIBLE COUPLINGS AND THEIR MOUNTING BOLTS

Summary of the Doctoral Thesis

Scientific supervisor
Associate Professor Dr. sc. ing.
PAVEL GAVRILOV

Consultants
Dr. sc. ing. ALEKSANDRS BOIKO
Dr. sc. ing. JĀNIS EIDUKS

RTU Press
Riga 2024

Gorbačovs, D. Failure Study of Rubber-Cord Flexible Couplings and their Mounting Bolts. Summary of the Doctoral Thesis. – Riga: RTU Press, 2024. – 56 p.

Published in accordance with the decision of the Promotion Council "P-22" of 7 december 2023, Minutes No. 04030-9.16.1/13.

Cover photo by Pjotrs Sokolovs

The research was supported by the European Social Fund within the Project No. 8.2.2.0/20/I/008, "Strengthening of PhD students and academic personnel of Riga Technical University and BA School of Business and Finance in the strategic fields of specialization" of the Specific Objective 8.2.2, "To Strengthen Academic Staff of Higher Education Institutions in Strategic Specialization Areas" of the Operational Programme "Growth and Employment".

https://doi.org/10.7250/9789934370281
ISBN 978-9934-37-028-1 (pdf)

DOCTORAL THESIS PROPOSED TO RIGA TECHNICAL UNIVERSITY FOR THE PROMOTION TO THE SCIENTIFIC DEGREE OF DOCTOR OF SCIENCE

To be granted the scientific degree of Doctor of Science (Ph. D.), the present Doctoral Thesis has been submitted for defence at the open meeting of RTU Promotion Council on February 23, 2024 at 13.00 at the Faculty of Civil and Mechanical Engineering of Riga Technical University, 6B Ķīpsalas Street, Room 513.

OFFICIAL REVIEWERS

Asoc.profesor Dr. habil. sc. ing Vladimirs Šestakovs,
Riga Technical University

Profesor Dr. habil. sc. ing. Marijonas Bogdevičius,
Vilnius Gediminas Technical University, Lithuania

Profesor Dr. sc. ing. Valeriy Kuznetsov
Railway Research Institute, Poland

DECLARATION OF ACADEMIC INTEGRITY

I hereby declare that the Doctoral Thesis submitted for review to Riga Technical University for promotion to the scientific degree of Doctor of Science (Pf. D) is my own. I confirm that this Doctoral Thesis has not been submitted to any other university for promotion to a scientific degree.

Dmitrijs Gorbačovs ……. (signature)

Date: ……

The Doctoral Thesis has been written in Latvian. It consists of an Introduction, 3 chapters, Conclusions, 198 figures, 51 tables, and 12 appendices; the total number of pages is 207, including appendices. The Bibliography contains 89 titles.

LIST OF ABBREVIATIONS

C – carbon
Mn – manganese
Si – silicon
V – vanadium
Cr – chromium
N – nitrogen
P – phosphorus
S – sulfur
Al – aluminum
Cu – copper
Ni – nickel
Ti – titanium
W – tungsten
Mo – molybdenum
Co – cobalt
Pb – lead
Zr – zirconium
HNO_3 – nitric acid solution
HB – hardness values according to Brunel
EMU – Electric Multiple Unit
ER1 – Riga electric train Type 1
ER2 – Riga electric train Type 2
ER2T– Riga electric train Type 2 with recuperative–rheostat braking
ЭР2Р – Riga electric train Type 2 with rheostat braking
ЭР2Т – Riga electric train Type 2 with recuperative–rheostat braking
ЕПЛ2 – Lugansk electric train Type 2
ЭТ2 – Torzhok electric train Type 2
ЭР9 – Riga electric train Type 9
ЕПЛ9 – Lugansk electric train Type 9
ЭД9 – Demikhov electric train Type 9
DR1A – Riga diesel train Type 1
ТГМ4 – Mamevru diesel locomotive with hydraulic transmission, Model 4
ТГМ – shunting diesel locomotive with hydraulic transmission, Model 6
ТЭМ – shunting diesel locomotive with electric drive, Model 2
TA-2 – Type 2 maintenance
TA-3 – Type 3 maintenance
TR-1 – Type 1 periodic repair
TR-2 – Type 2 periodic repair
TR-3 – Type 3 periodic repair
TR-3+ – Type 3 periodic repair with service life extension
VR – intermadiate overhaul
GR – main overhaul
FEM – Finite Element Modeling
LDz – State Joint Stock Company “Latvijas dzelzceļš”

CONTENTS

INTRODUCTION

Today, various types of couplings are used in mechanical engineering. A coupling made of highly elastic silicone, rubber, or rubber with reinforced fibers and a steel cord is used for the transmission of the rotational moment between the units exposed to significant dynamic, vibrating, and shock loads. Couplings of this type are designed to compensate for significant angular, axial or radial misalignments. The manufacturer indicates the maximum possible deviations in the product's passport and standard. Couplings with a highly flexible U or toroidal profile shell are used in various drives: in construction machinery and road construction equipment, machine building workbenches, rolling and drilling equipment, pump units, in transport – the rolling stock of multiple unit trains, as well as in the power drive of various types of ships.

Every year in Europe, a significant number of unplanned repairs of industrial equipment are recorded in connection with the failure of the flexible coupling (rubber cord shell). A failure of a flexible rubber cord coupling leads to the shutdown of industrial equipment or traction rolling stock for unscheduled repairs. In turn, unplanned repairs require funding to restore the equipment's operability. On average, the price of one unplanned repair consists of the price of the flexible coupling itself, the replacement of the unit connected to it, as well as the downtime of production equipment. In Latvia, in the period from 2012 till 2021, the rolling stock of JSC "Pasažieru vilciens" has had 101 cases of failure of the flexible rubber cord coupling. The financial losses to replace the damaged coupling averaged 575–594 euros, depending on the type of coupling. Due to this, there is a need to discover the cause of the failure timely and introduce modern technical solutions, with the aim of reducing the number of unplanned repairs and financial expenses related to the failure of the rubber cord coupling. Therefore, after analyzing the situation, a calculation methodology was developed and the influence of external factors on the side surface of the flexible coupling was evaluated. The methodology was developed by taking as an example the flexible coupling traction gear of JSC "Latvijas dzelzceļš" EMU rolling stock with a toroidal profile casing installed on ER2 series EMU car, and a U-shaped profile casing installed on ER2T series EMU car.

Research aim

The aim of the research: To reduce failures of rubber-cord couplings and their fastening bolts and to development a methodology to reduce the likelihood of this phenomenon.

Research tasks

1. Collect statistical data on the failure of rubber-cord couplings and bolts and systematize them.
2. Develop a methodology for researching failures of the rubber-cord coupling and its fastening bolts and carry out approbation.
2. Experimentally determine the material properties of the rubber-cord coupling and calculate the material properties at operating, critical, and breaking loads.

3. Create a calculation model of the flexible element of the rubber-cord coupling in the modeling program package.
4. Develop a shock-vibration load monitoring device for the fastening bolts of the rubber-cord coupling.
5. Develop recommendations for reducing the failure of rubber-cord couplings and their fastening bolts.

Research methods

1. Experiments were carried out on determining the material properties of rubber-cord fragments and the surface rubber layer of rubber-cord couplings under uniaxial tension.
2. Finite element modeling was used in the SolidWorks Simulation environment, applying nonlinear highly elastic material models.
3. In the SolidWorks Simulation environment, studies of the modal shapes, frequencies, and stress-deformation state of the coupling shells were carried out in order to evaluate the causes of their failure.
4. In order to assess the causes of the breakdown of the coupling fastening bolts, dynamic and static tensile tests of the bolts were performed, as well as microstructural and chemical analysis of the bolt material.

Scientific novelty of the Thesis

1. A methodology has been developed, for the timely detection of failures of the rubber-cord coupling casings and their fastening bolts, which are operated under the conditions of Latvian railways.
2. A computer model was developed in the SolidWorks Simulation environment, which, using the Mooney–Rivlin method, allows to estimate the impact of the load on the coupling and its maximum critical values, and dangerous frequencies and stress values at different speed ranges.
3. A shock-vibration device has been invented, which makes it possible to continuously accumulate and analyze data on the impact force to the bolts during the operation of the vehicle.

Reliability of the obtained result

The research results were evaluated and compared with the results of other authors and with the data obtained by unilateral deformation of several coupling shells in the course of full-scale experiments. The reliability of the experimental data was ensured by the accuracy of the measurements and comparison with the data of the normative documentation.

Practical significance of the research

The recommendations, which have been developed on the basis of the conducted studies, will allow to reduce the failure of the rubber-cord coupling in operation.

With the help of the developed shock and vibration force control devices of bolted fasteners, data on the impact force can be constantly collected and analyzed in order to reduce the number

of unplanned repairs of railway rolling stock or vehicles of other industries, as well as to reduce the number of accidents.

Approbation of the research results

The Thesis results have been reported and discussed at several scientific conferences in Latvia and abroad.

1. 19th International Scientific Conference "Economic Science for Rural Development", Jelgava, Latvia, 2020, the Latvia University of Life Sciences and Technologies.
2. 20th International Scientific Conference "Engineering for Rural Development", 26–28 May 2021, Jelgava, the Latvia University of Life Sciences and Technologies.
3. IEEE 9th Workshop "Advances in Information, Electronic and Electrical Engineering", Riga, Latvia, 2021.
4. 2020 IEEE 8th Workshop "Advances in Information, Electronic and Electrical Engineering", Vilnius, Lithuania IEEE 2020.
5. XIII International Scientific Conference "Transport Problems", Poland, Katowice – Sulejów. Silesian University of Technology, 2021.
6. Proceedings of the 10th International Scientific Conference "Rural Development", Kaunas, Lituania, 2021, Aleksandras Stulginskis University.
7. 26th International Scientific Conference "Transport Means", Kaunas University of Technology 2022.

Publications

1. Gavrilovs, P., Gorbačovs, D. Hardness Testing and the Chemical Composition Analysis of the Er2 and Er2t Series EMUs Traction Transmission Rubber-Cord Coupling Bolts. 19th International Scientific Conference "Economic Science for Rural Development", pp. 326–330, Jelgava Latvia, 2020, the Latvia University of Life Sciences and Technologies. ISSN 1691-5976.
2. Gavrilovs, P., Eiduks, J., Gorbačovs, D. Determination of the Causes of the Series ER2T Electric Multiple Unit Trains Traction Gear Rubber-Cord Shell Damage. 20th International Scientific Conference "Engineering for Rural Development", pp. 281—287, 26—28 May 2021, Jelgava, the Latvia University of Life Sciences and Technologies. ISSN 1691-5976.
3. Gorbačovs, D., Mihailovs, F., Eiduks, J. Analysis of the Formation of Defects in the Microstructure of the M-24 Bolts of the Rubber-Cord Coupling at Various Ranges of Mileage of Electric Trains Motor Cars. 2021 IEEE 9th Workshop "Advances in Information, Electronic and Electrical Engineering", pp. 1–4, Riga, Latvia, 2021. ISBN 978-1-6654-6713-1.
4. Gorbačovs, D., Gavrilovs, P., Eiduks, J., Strautmanis, G. Failure Analysis of Rubber-Cord Couplings of ER2 Series Electric Trains. 22th International Scientific Conference "Engineering for Rural Development", pp. 313—320, 24–26 May 2023, Jelgava, Latvia, 2023, the Latvia University of Life Sciences and Technologies. ISSN1691-5976.

5. Gorbačovs, D., Gavrilovs, P., Eiduks, J. Determination of the Metal Structure, Testing of Hardness of the Fastening Bolts of the Rubber-cord Coupling for Traction Gear of Electric Trains of the ER2 Series. 2020 IEEE 8th Workshop on Advances in Information, Electronic and Electrical Engineering, pp. 42—45, Vilnius, Lithuania, 2020. ISBN 978-1-6654-3087-6.
6. Gavrilovs, P., Eiduks, J., Gorbačovs, D. Determination of the metal structure, analysis of the chemical composition, testing of hardness and determination off static breaking stresses of the fastening bolts of the rubber-cord coupling for traction gear of electric trains of the ER2t series. XIII International Scientific Conference "Transport Problems", pp. 214–226, Poland, Katowice – Sulejów. Silesian University of Technology, 2021. ISBN 978- 83- 959742-1-2.
7. Mihailovs, F., Eiduks, J., Gorbačovs, D. Reducing the Number of Unscheduled Repairs of Traction Gear of EMU Trains by Introducing Modern Technical Solutions, Proceedings of the 10th International Scientific Conference Rural Development, pp. 113—117, Kaunas, Lituania 2021, Aleksandras Stulginskis University. ISSN 2345-0916.
8. Gavrilovs, P., Eiduks, J., Gorbačovs, D. Determination of the Chemical Composition and Impact Strength of the M-24 Bolts for Fastening the Rubber-Cord Coupling of EMU Trains, 26thInternational Scientific Conference "Transport Means", pp. 360—365, Kaunas University of Technology, 2022. ISNN 1822-296X.
9. Gavrilovs, P., Ivanovs, V., Gorbačovs, D. Study of Damage to VAE Cross Crossing. *Наука и техника Казахстана*, 2022, No. 1, pp. 142–154. ISSN 2788-8770. Available from: doi:10.48081/NJAY4790 ISSN 2788-8770. http://stk.tou.edu.kz/storage/journals/132.pdf.

1. OVERVIEW OF THE RESEARCH

Until now, various flexible couplings have been used to compensate the loads between the shafts. In mechanical engineering, the group of flexible couplings includes various coupling designs, insert-fingers, couplings with a flexible element in the form of a star, toroidal form and others. In the shafts of devices in the connection area of this type of couplings, there usually are axial, radial, and angular displacements. Therefore, the joints are subjected to significant mechanical and thermal loads. Such loads often cause damage to the connections between the elastic elements and the fastening elements.

- **Classification of rubber-cord couplings**

Rubber-cord couplings are widely used in modern mechanical engineering; they are designed for torque transmission between units from one shaft to another. Flexible couplings are subjected to significant vibration, dynamic and shock loads during operation over a wide range of scales. Flexible couplings reduce hits and shocks and serve as a safeguard against resonant torsional vibrations that occur as a result of uneven rotation, allowing relatively large displacements of the axes of the connected shafts.

Various types of flexible couplings are known in mechanical engineering, the design of which has several features:

- flexible pin and bush coupling;
- flexible coupling with a flexible element in the shape of a star;
- flexible couplings with toroidal rubber cord.

1.1. Damage analysis of the rubber-cord couplings and their fastening bolts in the Latvian railway

The failure data of the rubber-cord coupling and its fastening bolts for the period from 2012 to 2021 are shown in (Fig. 1.1).

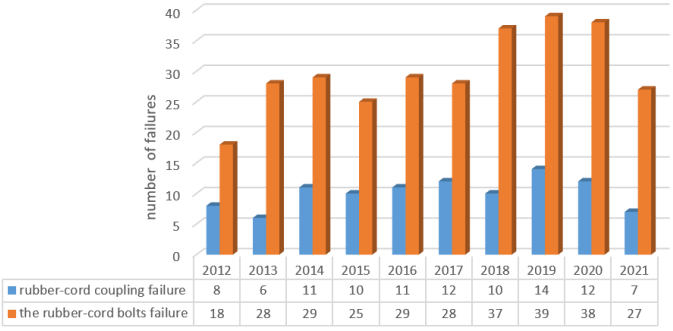

	2012	2013	2014	2015	2016	2017	2018	2019	2020	2021
rubber-cord coupling failure	8	6	11	10	11	12	10	14	12	7
the rubber-cord bolts failure	18	28	29	25	29	28	37	39	38	27

Fig. 1.1. ER2 and ER2T rubber-cord coupling and rubber cord coupling bolt failures.

In DR1A diesel trains, for the same time period from 2012 to 2021, 6 cases of rubber cord coupling failures and 14 cases of fastening bolt failures were detected. Data on the number of failures are given in (Fig. 1.2).

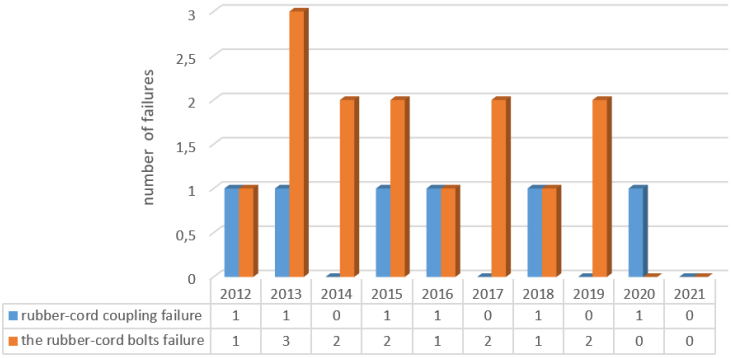

	2012	2013	2014	2015	2016	2017	2018	2019	2020	2021
rubber-cord coupling failure	1	1	0	1	1	0	1	0	1	0
the rubber-cord bolts failure	1	3	2	2	1	2	1	2	0	0

Fig. 1.2. DR1A rubber-cord coupling and fastening bolt failures.

Analyzing the provided statistical data shown in Figs. 1.1 and 1.2, it was found thatthe most frequent breakdown of rubber-cord coupling and fastening bolts occurs in electric trains (Fig. 1.3).

Fig. 1.3. Example of rubber-cord coupling layer rupture.

Accordingly, the question arises, why do rubber-cord coupling failures occur? And is this problem relevant in the world?

Therefore, the current situation related to the data on the time of operation of the coupling until failure was analyzed – the effect of various forces and stresses, the effect of temperature, as well as the effect of shaft deviations on the coupling. Taking into account the mentioned effects, a new methodology was developed for calculating and evaluating the influence of external factors on the casing of a flexible coupling. The methodology was developed using an available example of traction drive connections with a toroidal casing in the rolling stock of a Latvian railway motorcar.

2. DEVELOPMENT OF THE METHODOLOGY FOR REDUCING THE NUMBER OF FAILURES OF RUBBER-CORD COUPLINGS AND THEIR MOUNTING BOLTS

The purpose of the methodology developed by the author is to reduce the number of failures of the rubber-cord couplings and their fastening bolts, to determine in time the causes of damage to the bolts of the flexible coupling shell, and to develop measures to achieve a reduction in the number of failures of couplings and their bolts. The methodology for preventing the failure of the rubber-cord coupling and its bolt fastening consists of 10 steps.

1. Summarizing of statistical data on damage zones.
2. Control of warming up temperature parameters.
3. Rubber-cord coupling hardness test.
4. Rubber-cord coupling dimensions check.
5. Calculation of breaking forces of rubber-cord couplings.
6. Measurement of deviations of the rubber-cord couplings.
7. Frequency analysis of rubber-cord couplings.
8. Studies of rubber-cord coupling material properties.
9. Development of a rubber-cord model in the FEM software package
10. Determining bolt damage by various methods.

2.1. Summary of statistical data on damage zones

The surface of the coupling damage occurring in operation was determined and the distance from point A of the fastening disk to the damage place, point B, was measured (Fig. 2.1). Failure statistics was collected for more than N cases.

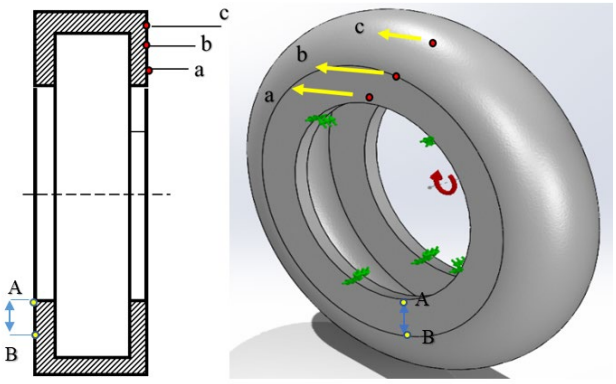

Fig. 2.1. Visual inspection of the rubber-cord coupling places:
a – lower part; b – middle part; c – upper part.

After visual inspection, areas of failure were identified, indicating the presence of problem areas in the rubber-cord coupling that require investigation. If the rubber-cord coupling is broken or damaged during operation, it must be replaced.

2.2. Control of warming up temperature parameters

Control of the heating temperature of the rubber-cord coupling as part of the technical service system must be carried out immediately after the production equipment has stopped. In order to perform temperature control, it is necessary to know the maximum allowable limit of heating temperature of the rubber-cord coupling in operation. The limit temperature t_{max} of couplings is regulated by the ISO and EN standarts. Temperature measurements should be made:

- a – in the lower part of the rubber cord coupling;
- b – in the middle part of the rubber cord coupling;
- c– in the upper part of the rubber cord coupling.

The temperature is measured in the upper, middle and lower part of the coupling in five places around the coupling circle, at least 5–7 mm away from the previous temperature measurement. The temperature measurement locations are shown in Fig. 2.2.

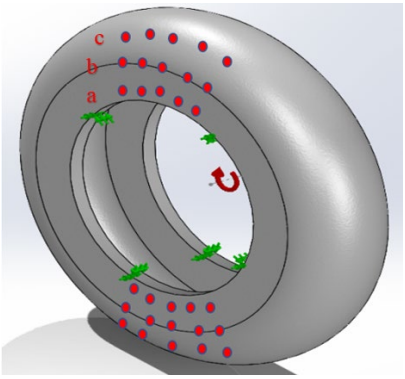

Fig. 2.2. Temperature and hardness measurement points:
a – lower part; b – middle part; c – upper part.

Temperature measurement locations are determined by the difference in diameters ($D - d$):

- a –10 % difference in the lower part;
- b –50 % difference in the middle part;
- c –90 % difference in the upper part.

The heating temperature test was performed for N rubber-cord couplings at 30 points $t_1 \ldots t_{30}$ (Fig. 2.2) from both sides and the average value of the heating temperature was determined, Eq. (2.1).

$$t_{vid} = \frac{\sum_{i=0}^{30} t_i}{30}, \quad (2.1)$$

where t_i is the heating temperature, °C

Check the compliance with the standard data and the average determined temperature with the maximum allowable t_{max}, Eq. (2.2).

$$t_{vid} < t_{max} \quad (2.2)$$

The periodicity of coupling warm-up temperature parameters control should be performed depending on the operating temperature conditions:

- –20 °C to 0 °C – once every 6 months;
- 0 °C to +20 °C – once every 6 months;
- +21 °C to +25 °C – once every 3 months;
- +26 °C to +30 °C – once a month;
- +31 °C to +35 °C – once a week.

.

2.3. Rubber-cord coupling dimensions check

In operation, the following geometric dimensions of the coupling are determined:

- outer surface diameter *D*, mm;
- inner seat diameter *d,* mm;
- thickness of the upper part *δ,* mm;
- side wall thickness δ_1, mm.

When measuring the rubber-cord coupling, it is necessary to know the limit values of the coupling sizes *D; d; δ;* δ_1 in permissible operation. Measurements must be performed on non-working equipment as part of system maintenance. Couplings size control must be carried out and *D, d,* and δ_1 must be determined (Fig. 2.3 a). The dimension, δ, was used for force P_c calculations. *D, d,* and δ_1 were compared with standard data D_{st}, d_{st}, and δ_{1st}:

- $D_{st} < D < D_{st}$;
- $d_{st} < d < d_{st}$;
- $\delta_{1st} < \delta_1 < \delta_{1st.}$

To accurately determine the diameter of the coupling, two measurements should be taken horizontally and vertically at an angle between the measuring plates of 90º. The measurement locations of geometric dimensions are shown in Fig. 2.3.

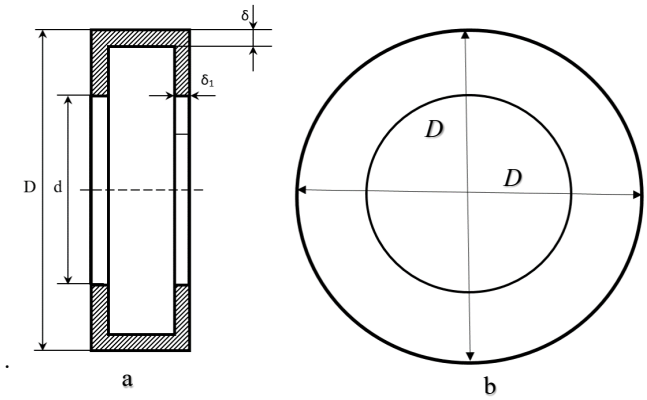

Fig. 2.3. Determining the geometric dimensions:
a – coupling size control; b – test on eccentricity.

The measurements of coupling diameter, D and d, and side surfaces, δ and δ_1, should be performed in three places along the coupling circle. The obtained coupling measurement results are compared versus the data of the ISO, EN, and DIN standards, which regulate the limit sizes of the rubber-cord coupling allowed in operation.

As part of the methodology, it was proposed to selectively control the dimensions of new couplings before putting them into operation. For the couplings in service, the geometric dimensions are checked depending on the rotation frequency:

- up to 700 rpm – once a year;
- from 701 to 1500 rpm – every six months;
- from 1501 to 1800 rpm – every three months;
- from 1801 to 2000 rpm – once a month.

According to the measurement results, if the size of the coupling complies with standards ISO, EN, and DIN, the coupling is allowed to operate; if the size of the coupling does not comply with ISO, EN, and DIN standard requirements, then this coupling must be withdrawn from operation.

The geometric dimensions of the couplings are further used to calculate the forces and stresses acting on the coupling during operation methodology (step 2.5).

2.4. Testing the hardness of the rubber-cord coupling

The rubber-cord coupling hardness is regulated by standard ISO, EN, and DIN. According to the standard, the hardness of the rubber-cord coupling is determined by the Shore A method and should be within the range of 50.0–65.0 conditional units. The hardness measuring device must ensure the measurement accuracy at the ambient temperature range from –30 °C to +60 °C. Measurement of coupling hardness should be done at different temperature ranges:

- –20 °C;
- 0 °C;
- +20 °C;
- +60 °C.

Hardness measurements in the upper, middle and lower parts of the coupling shall be made at least 5–7 mm away from the location of the previous temperature measurement. The hardness measurement locations are shown in Fig. 2.2.

Hardness measurement locations are determined by the difference in diameters ($D - d$):

- a –10 % difference in the lower part;
- b –50 % difference in the middle part;
- c –90 % difference in the upper part.

It is necessary to take five hardness measurements in each temperature range:

- in the lower part of the rubber-cord coupling;
- in the middle part of the rubber-cord coupling;
- in the upper part of the rubber-cord coupling.

Te hardness of N rubber-cord couplings should be tested at 30 points and $C_1 ... C_{30}$ (Fig. 2.2) from each side of the coupling and the average value calculated using Formula (2.3).

$$C_{\text{vid}} = \frac{\sum_{i=0}^{30} C_i}{30}, \tag{2.3}$$

where C_i is hardness, conditional units.

The average determined C_{vid} is checked with maximum permissible $C_{\max}$, Eq. (2.4).

$$C_{\text{st min}} < C_{\text{vid}} < C_{\text{st max}} \tag{2.4}$$

Hardness measurements are performed depending on the temperature conditions under which the rubber-cord coupling operates:

- from –20 °C to 0 °C, once a month;
- from +1 °C to +20 °C, once every 3 months;
- from +21 °C to +40 °C, once a month;
- from +41 °C to +60 °C, once a week.

If the hardness of the clutches does not meet the requirements of regulatory documentation, then the coupling must not be put into operation, but the existing coupling must be replaced with a new one.

If the conditions are not met, then the rubber-cord coupling must be replaced. If the conditions according to the steps of the methodology are met, then we move on to point 5 of the methodology.

2.5. Calculation of the disintegration forces of a rubber-cord coupling

If coupling failures occur during operation, but the geometric dimensions, hardness parameters and heating temperature of the coupling meet the requirements of the ISO, EN, and DIN standards, then in order to identify the causes of the coupling failure, it is necessary to perform force, stress,

and torque calculations. The forces, stresses and torque acting on the coupling and their maximum values under operating conditions should be determined.

The impact of the centrifugal force, P_c; P_{c1}, is shown in Fig.2.4.

According to step 2.5 of the methodology., it is necessary to determine the action of forces in order to identify the dangerous operating modes of the rubber-cord coupling at different speed ranges.

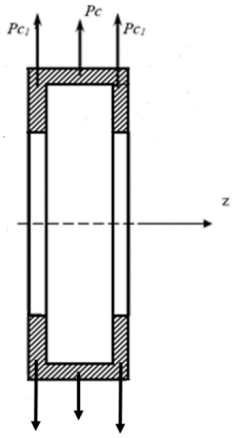

Fig. 2.4. Centrifugal force acting on the coupling.

The resultant specific centrifugal force acting on the coupling N/m:

1. Acting in the center of the coupling

$$P_c = \int_0^{b-2\delta} q \cdot dz = \int_0^{b-2\delta} \rho \cdot \delta \cdot \frac{D-\delta}{2} \cdot \omega^2 \cdot dz = \rho \cdot \delta \cdot \frac{D-\delta}{2} \cdot \omega^2 \cdot (b - 2 \cdot \delta), \quad (2.5)$$

where

ω – angular speed, rad/s;

q – intensity of centrifugal force on the coupling side surface, N/m^2;

ρ – rubber density, kg/m^3;

δ – thickness of the upper surface of the coupling, mm;

b – coupling thickness, mm;

D – diameter of coupling, mm.

2. Acting on the side surface:

$$P_{c1} = \int_0^{\delta_1} q_1 \cdot dz = \int_0^{\delta_1} \rho \cdot \frac{D^2 - d^2}{4} \cdot \omega^2 \cdot d \cdot dz = \rho \cdot \frac{D^2 - d^2}{4} \cdot \omega^2 \cdot d \cdot \delta_1, \quad (2.6)$$

where

ω – angular speed, rad/s;

ρ – rubber density, kg/m^3;

q_1 – centrifugal force intensity on the side surface of the coupling, N/m^2;

δ_1 – coupling side thickness, mm;

b – coupling thickness, mm;

D – diameter of coupling, mm.

3. The ratio of the torsional displacement tangential stresses to the friction point τ and determining the ratio to the coupling mounting flange $\tau_к$.

- The tangential stress of coupling displacement relative to the coupling mounting flange (shown in Fig.2.5).

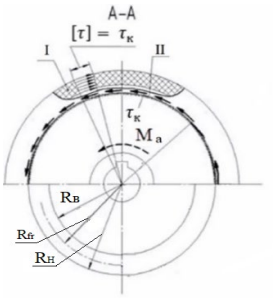

Fig. 2.5. Effect of torsional shear tangential stress:
$R_в$ – inner radius of the ring; $R_н$ – outer radius of the ring; R_{fr} – friction radius;
$\tau_к$ – torsional shear tangential stress in relation to the coupling mounting flange;
M_a – torque of the rotor shaft; I – torsion area; II – torsional displacements of the anchor shaft.

- The tangential stress of coupling displacement relative to the coupling mounting flange:

$$\tau_k = \frac{M_a}{\frac{\pi D^4}{32}\left(1-\frac{d^4}{D^4}\right)}\frac{D}{2} = \frac{16 \cdot M_a}{\pi D^3\left(1-\frac{d^4}{D^4}\right)} \leq [\tau], \qquad (2.7)$$

where

M_a – traction motor torque, k N m;

D – the outside diameter of the ring, mm;

d – the inner diameter of the ring, mm;

ρ – friction radius, mm;

$[\tau]$ – allowable tangential stress 0.7–0.75 MPa [27].

The obtained tangential shear stress calculation results were compared with the permissible tangential stress.

Torque is determined by Formula (2.8).

$$M_a = \frac{30 \cdot P}{\pi \cdot n}\eta, \qquad (2.8)$$

where

P – traction motor power – k W;

π = 3.14;

n – traction motor speed, rpm;

η – traction motor efficiency 86–92 % [22].

In addition, in accordance with Formulas 2.11 and 2.12, the torsional shear tangential stress τ_k and the moment Ma is determined at low speeds from 0 rpm to 200 rpm, and determine the action of the centrifugal force P_c at high speeds from 500 rpm to 2000 rpm.

The numerical value of stress and moment forces is determined with an accuracy of one hundredth (0.00) of the calculated units.

The calculated value of the force P_c and the effect of the moment M_a are further used in the FEM modeling program.

2.6. Measurement of deviations of the rubber-cord coupling

The permissible values of axial, radial and angular deviations of couplings are regulated by the ISO, EN, and DIN standard and are measured:

a – in the radial direction;

b – in the axial direction;

c – in the angular direction.

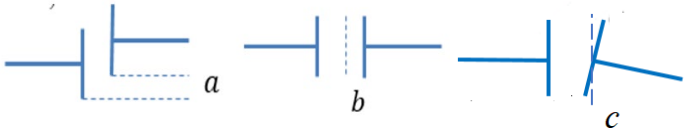

Fig. 2.6. Types of coupling deviations:
a – in the radial direction; b – in the axial direction; c – in the angular direction.

Determining the coupling deviations should be done on non-working equipment as part of the maintenance procedure. Deviation measurements for N couplings should be carried out in three places, shown in Fig. 2.7, along the coupling circle:

- in the upper part of the coupling α – 0°;
- in the middle part of the coupling β – 90°;
- in the lower part of the coupling ϒ – 180°.

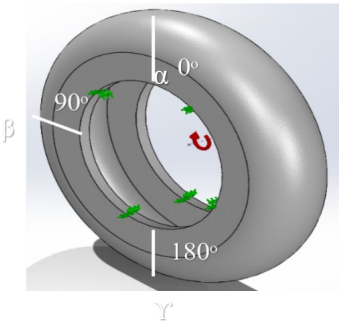

Fig. 2.7. Rubber-cord coupling measurement locations.

Each coupling should the following measurements:

- radial $a_\alpha, b_\alpha, c_\alpha$;
- axial $a_\beta, b_\beta, c_\beta$;
- angular $a_\gamma, b_\gamma, c_\gamma$.

The obtained measurement data should be compared with standard data:

$$a_\alpha, b_\alpha, c_{\alpha,} a_\beta, b_\beta, c_{\beta,} a_\gamma, b_\gamma, c_\gamma < a_{\text{st}}, b_{\text{st}}, c_{\text{st}}.$$

The obtained measurement data of axial, radial and angular deviations are used for modeling in the FEM software environment to determine the influence of deviations on the safe operation of the rubber-cord coupling.

2.7. Research on material properties of rubber-cord coupling

In order to perform the frequency analysis of the rubber-cord coupling, it is necessary to determine for N samples:

- the rubber-cord coupling mass, *M*;
- the coupling stiffness coefficient, *F*;
- self-frequencies of the coupling resonance, ω.

Determining the rubber cord coupling mass was done by weighing, using scales with an accuracy of ±50 g.

Coupling stiffness *K* was determined:

$$K = M_a/\varphi, \qquad (2.9)$$

where M_a is torque, k N m, and φ is the turning angle, rad.

The self-frequencies of the coupling depend on the rigidity (the fastening method) and on the mass of the coupling, Formula (2.10):

$$\omega = (F/M)^{0.5}, \qquad (2.10)$$

where *F* is the coupling stiffness coefficient, H/m, and *M* is the coupling mass, kg.

To obtain results in hertz, Formula (2.14) must be divided by 2π:

$$\omega = (F/M)^{0.5}/2\pi, \quad (2.11)$$

where π is mathematical constant, $\pi = 3.14$.

Further, the study of resonance frequencies is used in the FEM modelling software in step 9 of the methodology in order to determine dangerous frequencies at which the amount of mass of a certain coupling participates in the oscillations.

2.8. Research on material properties of the rubber-cord coupling

The aim of the research is to determine the mechanical properties of the rubber-cord coupling material under different types of loads. Determining the material properties is carried out with a tensile test device under single-break and cyclic loads, with maximum loading of the areas subject to failure.

In order to determine the properties of the material, it is necessary to perform crushing and cyclic experiments of the rubber-cord coupling fragments. The coupling is divided into *N* similar parts, and *1/N* fragments are taken for smashing and cyclic experiments.

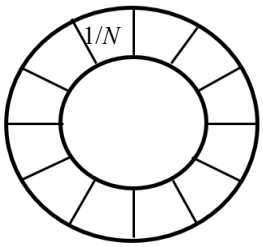

Fig. 2.8. Selection of sample sizes and shapes of the coupling casing fragments.

A series of N_i tests were carried out under single crushing and under cyclic loading to determine the material properties:

1) deformation – L_i, mm;
2) relative deformation – ε_i;
3) elastic modulus – E_i, MPa;
4) stress – σ_i, MPa;

According to the test results, to determine the dependence $\sigma = f(\varepsilon)$, the approximation should be performed:

$$\Sigma = f(\varepsilon) = a\varepsilon^n + b\varepsilon^{n-1} + k_0, \quad (2.12)$$

where σ is stress, MPa, ε is relative deformation, and *a, b,* and k_0 are coefficients.

Based on the test results, the dependence of the deformation on the stress was determined and with the results of approximation of the obtained data a mathematical model of the material was created. Next, based on the test results, the obtained material properties were used to create the

elastomer material model in the FEM environment and to form the material model in step 9 of the methodology.

2.9. Development of a rubber-cord coupling model in the FEM software package

In order to implement this step of the methodology, a software tool in the FEM package must be selected, in which the modeling was be performed (ANSYS, ABAQUS, MD ADAMS MEDINA, SOLIDWORKS). The most suitable tool for design, computational modeling and stress state analysis of elastomeric material was created and the model of FEM material was determined.

Data of material properties of the model from the methodology step 8 and the test results, the dependence of stress, σ, on the deformation, ε (σ=f(ε)), at single rupture and type of cyclic loading, was entered into the modeling program. The elastomer material models were selected from:

1) Mooney–Rivlin methods, $\sigma_{MR} = f(\varepsilon)$;
2) Blatz-Ko methods, $\sigma_{BL} = f(\varepsilon)$;
3) nonlinear elastic method (NLE), $\sigma_{NLE} = f(\varepsilon)$.

In FEM, a rubber-cord coupling material model was created for each of the elastomer material models listed above.

Modeling accuracy was identified:

$$\Delta_1 = \sum(\sigma_{MR} - \sigma)^2 \quad (2.13)$$

$$\Delta_2 = \sum(\sigma_{BL} - \sigma)^2 \quad (2.14)$$

$$\Delta_3 = \sum(\sigma_{NLE} - \sigma)^2, \quad (2.15)$$

where σ is stress after trial results, MPa, and $\sigma_{MR}, \sigma_{BL},$ and σ_{NLE} is stress after the modulation results, MPa.

A model was chosen $-\ \Delta_1; \Delta_2; \Delta_3 = \min$.

Further, with the selected material model, the modeling was performed of working condition parameters P_c, M_a, a_α, b_α, c_α, ω and with different modulation parameters the most heavily loaded areas of the rubber-cord coupling were determined. The obtained data were compared with P_c, M_a, a_α, b_α, c_α, ω, and limit values.

Based on the modeling results in the FEM software, the most stressed areas of the rubber cord coupling were determined

2.10. Determining the bolt damage by various methods

The purpose of this methodology step is to find and determine the causes of bolt failure. In order to determine the reasons for bolt failure, a number of tests were performed of bolts with different working time:

$$t_{eksp} = \sigma_t f(\Delta t), \quad (2.16)$$

where t_{eksp} is operating time, h; σ_t is breaking stress, MPa; and (Δt) is the time interval, h;

- crushing under static load P_c, for N samples;
- crushing under dynamic load P_d, for N samples;
- crushing under impact load a_k at different temperature ranges, for N samples;
- determining hardness, *HB,* for N samples;
- determining the chemical compositions of N samples for the presence of harmful impurities of phosphorus (P) and sulfur (S).

The purpose of the tests is to determine the reasons for the failure of the rubber-cord coupling bolts. The obtained test results should be compared with ISO and EN standard data.

The purpose of metallographic analysis is to obtain information about the structure of the material at the microscopic level by preparing a sample and analysing its surface.

3. APPROBATION OF THE METHOD USING THE EXAMPLE OF TOROIDALO RUBBER-CORD COUPLING

3.1. Investigation of the causes of the side surface destruction of the rubber-cord coupling

There were 21 cases of coupling damage in the period from September 2019 to 31 December 2021. Examples of the side surface disintegration of the rubber-cord coupling are shown in Fig. 3.1.

Fig. 3.1. Examples of the side surface disintegration of a rubber- cord coupling: a – sample 1; b – sample 2; c – determining the destruction zone sample 2.

During the period from September 2019 to 31 December 2022 there were 21 cases of disintegration of the side surface of the rubber-cord coupling:

- 1 (one) case is related to wear of the upper surface of the coupling caused by friction against the reducer mounting bolt;
- 20 cases are related to damage in the area of attachment of the casing to the flanges.

All 20 cases of failure of rubber-cord coupling are related to the crushing of the side surface. With a detected place of destruction – the coupling wall at a distance of 10–20 mm from the attachment point of the outer diameter disc.

3.2. The results of determining the heating temperature of the rubber-cord coupling

In order to determine the heating temperature of the rubber-cord coupling under real operating conditions, the author of the Thesis conducted three experimental trips with passenger trains: two trips with electric train No. 1307 and one trip with electric train No. 1342R.

According to the results of the test runs, it was established that the conditions for the coupling not to heat up more than + 75 ºC [21] are observed in the Latvian railway.

In total, the heating temperature was measured for 44 rubber-cord couplings.

3.3. Determining the geometric dimensions of coupling

The obtained measurement results were compared with DIN EN 13913:2003-08 [1] standard data and are shown in Table. 3.1.

Table. 3.1

Determining Geometric Dimensions of Coupling

Index name	Sample measurement indicators, mm		DIN EN 13913:2003-08, mm
	Sample 1	Sample 2	
The largest limit value of the diameter of the outer surface, *D*	$586.5^{+0.1}_{-0.1}$	$580.5^{+0.1}_{-0.1}$	580^{+2}
Inner buttock diameter, *d*	$354.5^{+0.1}_{-0.1}$	$354.8^{+0.1}_{-0.1}$	354^{+2}_{-2}
Side wall thickness, δ_1	$28.5^{+0.1}_{-0.1}$	$29.2^{+0.1}_{-0.1}$	30^{+2}_{-2}

Based on the results of measurements, it was found that all sizes of couplings, except the diameter *D* of the outer surface of sample 2, meet the requirements of the DIN EN 13913:2003-08 standard. In total, the overview of rubber-cord coupling samples measured during the technical service is 53 pieces. From the measurement results of 53 couplings, it was found that the outer surface diameter *D* of three couplings does not meet the standard requirements.

3.4. Determining the hardness according to the Shore A method depending on temperature

The research aims to determine the hardness at different temperature regimes. Hardness measurements were carried out in the RTU laboratory using a rubber hardness meter Elcometer 3120 Shore Dustomer A [10], the hardness test was performed in accordance with the requirements of the ISO 7619-1:2010 standard [7], the hardness measurement data of two rubber-cord coupling fragments were compared with ISO 14691:2008 standard data [8], the hardness measurements were made in four different temperature ranges:

- +60 °C;

- +22 °C;
- 0 °C;
- –20 °C.

According to the obtained measurement results, it was established:

- At a temperature of –20 °C, the measured hardness values of both couplings exceed the standard hardness parameters [8] by 6.4–11.9 conditional units.
- At a temperature of 0 °C, the measured hardness values of both couplings exceed the standard hardness parameters [8] by 3–6.4 conditional units.
- At a temperature of +22 °C:
    - for sample 1, two average measurement values exceed the standard hardness parameters [8] by 1.0–2.9 conditional units;
    - for sample 2, all average measurement values exceed standard hardness parameters [8] by 2.0–4.4 conditional units.
- At a temperature of +60 °C, the hardness values for both couplings were not exceeded.

Based on the results of hardness measurements, a significant increase in hardness was found during the winter period.

3.5. Calculation of breaking forces of rubber-cord coupling

In order to determine the causes of the breakdown in accordance with step 2.5 of the methodology of the rubber-cord coupling, calculations were made of the forces acting on the damage zones of the couplings during operation – forces P_c and P_{c1}, as well as tangential stress τ_k and torque M_a.

- **Determining the torque**

In the conditions of suburban traffic, with short track sections and with frequent stops of the electric train at stops, the maximum torque, M_a, is reached at low revolutions of the traction motor during the acceleration of the electric train. The maximum torque is determined by Formula (2.12).

According to the calculation results, torque M_a at five speed ranges is shown in Table 3.2.

Table 3.2

Torque Constant

EMU train speed, m/h	Traction motor speed, rpm	Torque M_a, N·m
5	64	1.74×10^4
10	129	8.65×10^3
20	258	4.32×10^3
40	517	2.15×10^3
120	1825	0.96×10^3

According to the calculation results, it was found that at 64 rpm, the loss of stability of the rubber-cord coupling occurs, which according to [21] occurs at 1.2×10^4 N m. Loss of rubber-cord coupling stability is the inability of the coupling to maintain its original position or shape.

- **Determining the centrifugal force**

Centrifugal force P_c and P_{c1} is determined according to Formulas (2.5) and (2.6), at 60 km/h and a maximum speed of 120 km/h.

Angular speed, ω:

- at speed 60 km/h = 72.24 rad/s;
- at speed 120 km/h = 191.07 rad/s.

The results of measuring the side surface of couplings are shown in Table 3.3.

Table 3.3

Determining the Coupling Parameters

Sample No	Thickness of the upper surface of the coupling, δ, mm	Coupling side thickness, δ_1, mm	Coupling thickness, b, mm
1	15.8	21.1	132.1
2	16.5	21.4	131.6
3	15.9	22.2	130.2

According to step 2.5 of the methodology, the forces acting on the rubber-cord coupling were calculated. The calculation data are shown in Table 3.4.

Table 3.4.

Calculation Results

Coupling parameters	Angular speed, rad/s	P_c, N/m	P_{c1}, N/m
Sample 1	72.24	7.80×10^3	1.05×10^4
	191.07	1.43×10^4	1.93×10^4
Sample 2	72.24	7.95×10^3	1.06×10^4
	191.07	1.44×10^4	1.95×10^4
Sample 3	72.24	7.61×10^3	1.02×10^4
	191.07	1.39×10^4	1.88×10^4

- **Determining torsional displacement tangential stresses**

In order to determine the torsional shear tangential stress τ_k, it is necessary to measure the coupling flanges. For this purpose, flange measurements of Samples 1 and 2 were made.. For Sample 3, the flange was not measured because the coupling is new and has not been in service. The measurement data are shown in Table 3.5.

Table 3.5

Coupling Flange Measurement Data

Sample No	The outside diameter of the ring, D, mm	Inner diameter of the ring, d, mm	Coupling pressure point for flange, friction radius, ρ, mm	Area of friction radius, $d\rho$, mm
1	$421.1^{+0.1}_{-0.1}$	$340.2^{+0.1}_{-0.1}$	$175.3^{+0.1}_{-0.1}$	$15.1^{+0.1}_{-0.1}$
2	$420.2^{+0.1}_{-0.1}$	$339.9^{+0.1}_{-0.1}$	$175.1^{+0.1}_{-0.1}$	$15^{+0.1}_{-0.1}$

Calculation results are shown in Table. 3.6.

Table 3.6

Results of couplings stress and force calculations

Sample No.	Traction motor speed, rpm	$\tau_к$, MPa
Sample 1	64	2.05
	129	1.02
	258	0.51
Sample 2	64	2.07
	129	1.03
	258	0.51

According to the calculation results, it was found that the maximum shear tangential stress in relation to the coupling mounting flange τ_k is reached at the moment of starting the electric train from the place, up to 64 rpm, when the maximum tangential stress is exceeded:

- Sample 1 – by 1.30 MPa;
- Sample 2 – by 1.32 MPa.

3.6. Measurement results of axial radial and angular deflection of rubber-cord coupling

When installing the coupling on the rolling stock, the deviations of the coupling during its installation must meet certain parameters, which are regulated [19]. According to [19], displacement measurements of rubber cord couplings are performed after restoration during repair TR-3 [20] in the upper part.

The data of the average value of the measurements (0°; 90°; 180°) are shown in Table 3.7.

Table 3.7

Coupling Angle Deviation Measurement Data 2020–2021

Coupling misalignment	Radial displacement, mm	Axial displacement, mm	Angular displacement, degrees
Average measured value	from 1 till 15 mm	from 2 till 16 mm	0° ± 4°
Maximum allowable value	15.0	20.0	4.0

As a result of the analysis of the measurement data of the parameter deviations indicated in Table 3.7, the following graphs were obtained (Figs. 3.2–3.4).

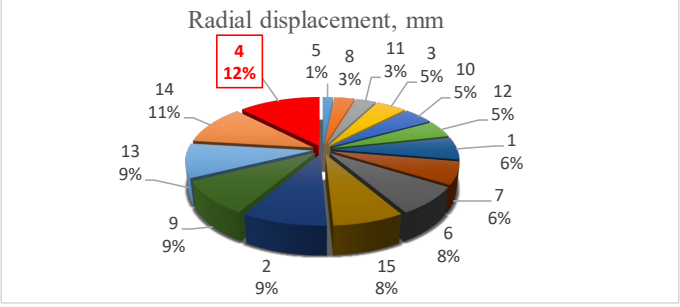

Fig. 3.2. Radial displacement of the shafts in percentage.

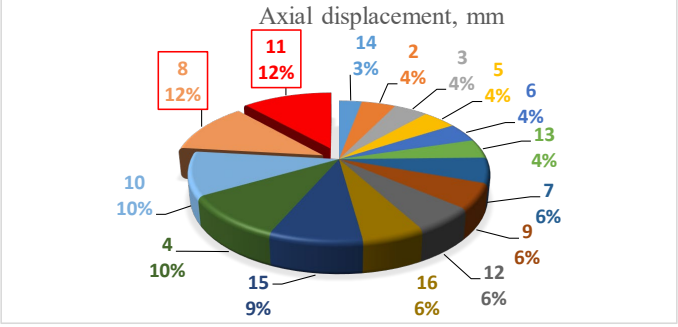

Fig. 3.3. Axial displacement of values in percentage.

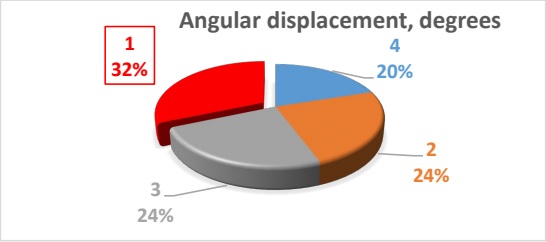

Fig. 3.4. Angular displacement measurements in percentage.

Analyzing the data of inclination angles, cases of significant deformations of flexible couplings in radial, axial, and angular directions were found.
As a result of the measurement data analysis, it was found that the most common occurrences in operation are:

1) deviation of 4 mm in the radial direction – 8 cases or 11.42 %;
2) deviation of 11 mm and 8 mm in axial displacement – 16 cases or 22.85 %;
3) deviation of 3 mm in angular displacement – 17 cases or 24.28 %.

When measuring the displacement of the shaft, it was found that on several wheelsets, the deviations of the shafts are significant in all three directions: the radial, axial, and angular.

3.7. Calculation of the elastic element of a rubber-cord coupling using FEM modeling software package

Experimental studies of the coupling shell were carried out to determine the working loads and maximum force loads of the coupling shell, under single uniaxial stretching and under cyclic stretching. Several elements were tested in the RTU laboratory. Then, during the trial, the optimal shape and dimensions of the coupling fragments were determined, fhe data is shown in Table 3.8.

Table 3.8

Measurements of Coupling Samples

Coupling samples	Thickness at base, mm	Thickness of the upper part, mm	Thickness at the point in disintegration place, mm	Thickness of the upper part, mm
Sample group 1, Fragments 1 and 4	65 ± 2	105 ± 1	20 ± 2	15.5 ± 1
Sample group 2, Fragments 2; 3; 5; 6	67 ± 2	96 ± 2	19 ± 2	15 ± 1

3.8. Results of tests on sample coupling shells

The nature of deformation changes for coupling fragments 2 and 5 from the first and second groups under cyclic loading is shown in Table 3.9.

Table 3.9.

Sequence of Loading of Fragments of the Coupling Shell

Load characteristics	Number of load cycles, pcs	Loading speed, mm/s
Operating loads	10	0.4
Sudden loads (until breaking)	20	0.8

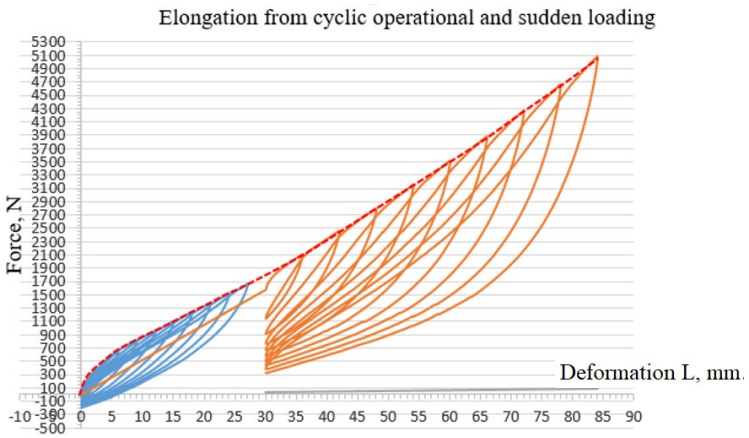

Fig. 3.5. Deformation graph of Fragments 2 and 5, depending on operational and sudden cyclic loads.

Cyclic load results show that when deforming the coupling shell fragment up to 25 mm, which is the critical value in operation, the force value reaches approximately 1500 N. For further deformation of the coupling shell fragment up to 80–90 mm, the effect of strengthening the material of the coupling shell is observed, so that with each new loading the load increases non-linearly and reaches 7500 N at a maximum deformation of 90 mm.

A comparison of the results of the one-way stretching test of coupling Fragments 1 and 4 at one-time stretching ($R^2 = 0.9991$) and coupling Fragments 2 and 5 at operation and extreme cyclic loads ($R^2 = 0.9995$) until disintegration are shown in Fig. 3.6.

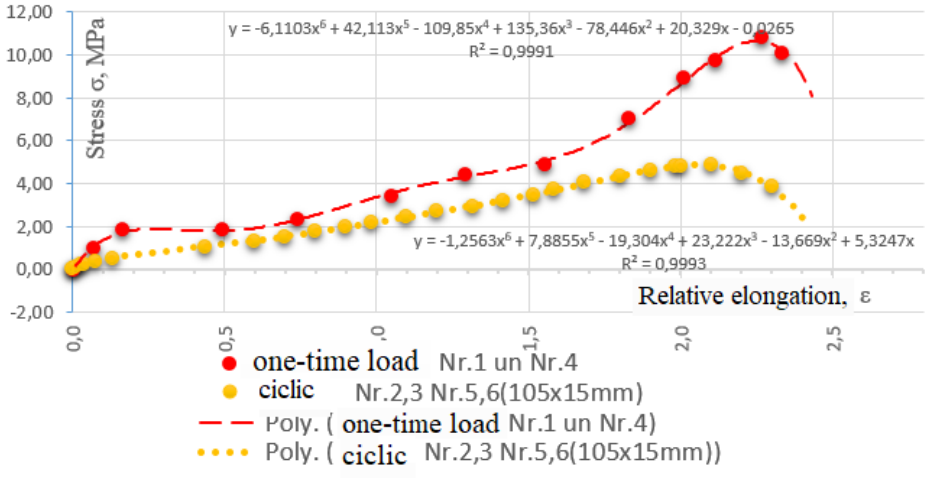

Fig. 3.6. Comparison of unilateral tensile test results.

According to the test results of the coupling fragments, the elastic moduli were calculated. At one-time stretching of Fragments 1 and 4, the calculated modulus of elasticity is 14 MPa. At cyclic operating loads of coupling Fragment 2, the calculated modulus of elasticity is 10 MPa.

3.9. SolidWorks program for creating a calculation model

In order to create a numerical model of the coupling material, a comparative analysis of the results of several tests was carried out.

Based on the obtained results, the evaluation of the mechanical properties of the rubber samples of the surface layer was done and the results for the coupling shell fragments under single stretching and cyclic stretching loads were calculated. Calculation data is shown in Tables 3.10–3.11.

Table 3.10

Average Result of One-time Stretching of Coupling Fragments 1 and 4

Limit of proportionality, MPa	Modulus of elasticity, MPa	Strength limit, MPa	Yield strength, MPa	Breakdown stress, MPa
$\sigma_{0.2}$	E	σ_b	σ_y	Fracture
0.98	14.73	10.86	2.38	10.13

Table 3.11

Cyclic loading of fragments No. 2 and No. 5

Limit of proportionality, MPa	Modulus of elasticity, MPa	Strength limit, MPa	Yield strength, MPa	Breakdown stress, MPa
$\sigma_{0.2}$	E	σ_b	σ_y	Fracture
0.102	15.24	4.87	0.50	3.88

According to the calculated material characteristics, a material calculation model from the coupling shell fragments was developed in the SolidWorks calculation program.

3.10. Modeling a fragment of the rubber-cord shell of the coupling

Next, the calculation model of the fragment of the coupling shell were developed, (Fig. 3.7). Variant calculations of coupling shell fragment were performed using various methods of material modeling and for various strains.

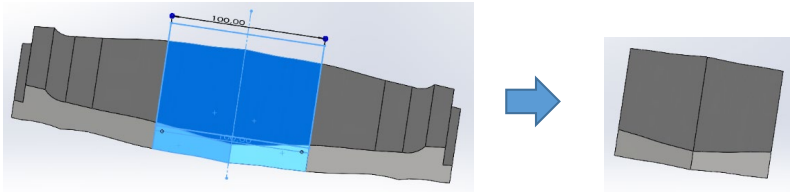

Fig. 3.7. Shell fragment model with a stretch area of 100 mm.

A complete model of a shell fragment with a zone from 100 mm to 220 mm subject to tension during testing and a modified calculation model of the shell for testing material models are shown in Fig 3.8.

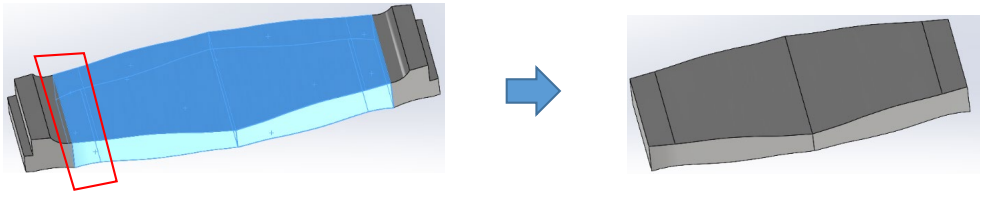

Fig. 3.8. Shell fragment model with a stretch area of 220 mm.

- **Superelastic material modeling using the Mooney–Rivlin method**

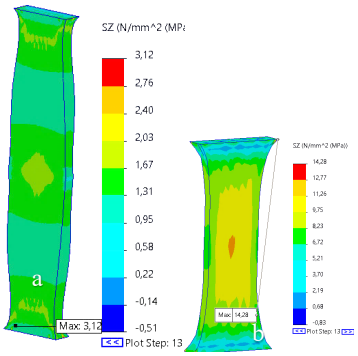

Fig. 3.9. Stretch pattern of superelastic material:

a – a 220 mm model at 135.9 mm extension; b – a 100 mm model at 135.9 mm extension.

The stress distribution on the vertical edge of the fragment of the superelastic material model according to the Mooney–Rivlin method is shown in Fig. 3.10.

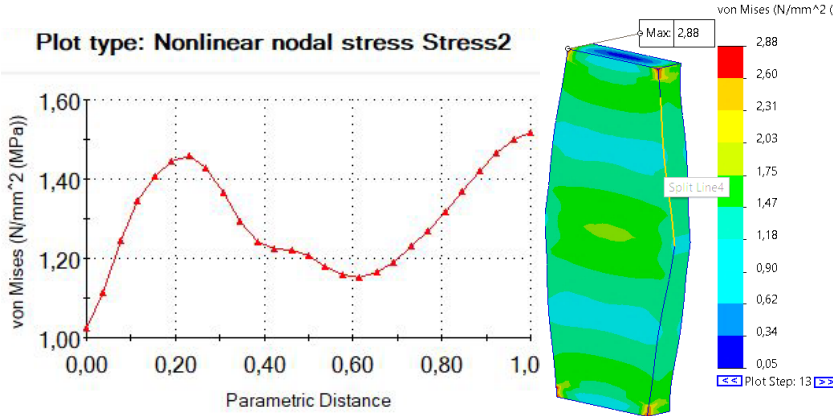

Fig. 3.10. Edge response from the anchorage to the mid-section of the 100 mm long fragment.

• **Superelastic material modeling using the Blatz method**

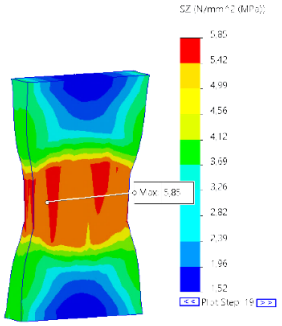

Fig. 3.11. Calculation of a 110 mm fragment for stretching to 66.06 mm.

The stress distribution on the vertical edge of the fragment of the superelastic material model according to the Blatz method is shown in Fig. 3.12.

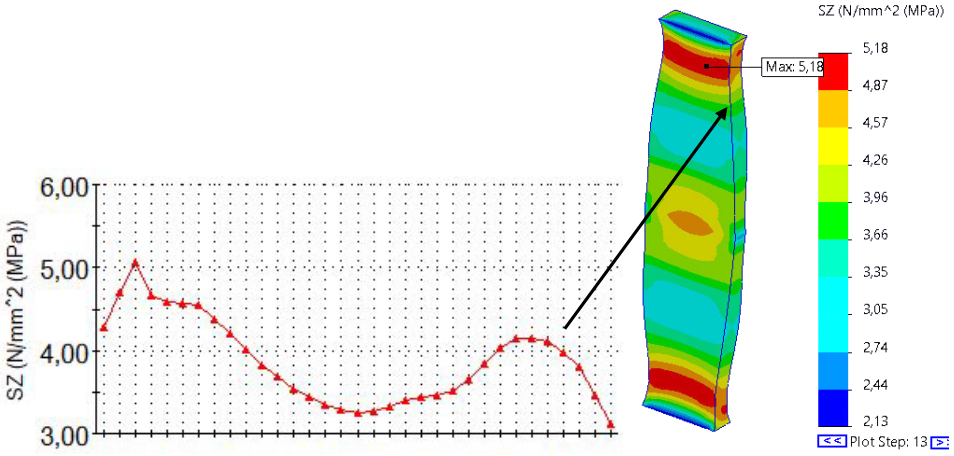

Fig. 3.12. The tension distribution from the fastening point to the middle part of the fragment is 100 mm.

• Superelastic material modeling using nonlinear elastic method (NLE)

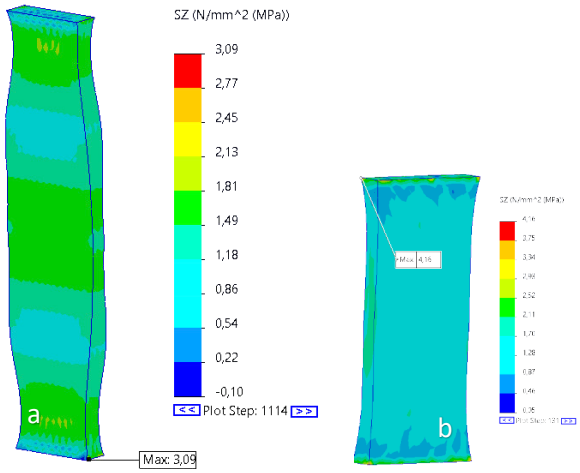

Fig. 3.13. Stress distribution according to the nonlinear elastic material model: a – model length is 220 mm; b – model length is 100 mm.

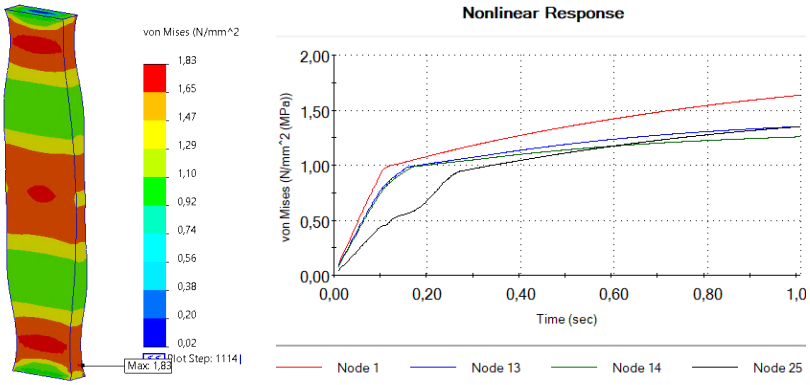

Fig. 3.14. Node response of the nonlinear model (sample length 220 mm).

It has been established that the Blatz method does not reflect the results of the experiments after reaching a 130–140 % deformation. Thus, for small deformations of the coupling shell, we can use both methods with appropriate material adjustment, but for deformations greater than 130 %, the Mooney–Rivlin method is used. For large deformations according to the Mooney–Rivlin method, it is necessary to add a third constant to the material model. Also, the diagrams of the two material models are different. Using the Blatz method, the deformation zone is expressed by the formation of a neck at the place of further disintegration of the shell fragment during stretching (Fig. 3.11).

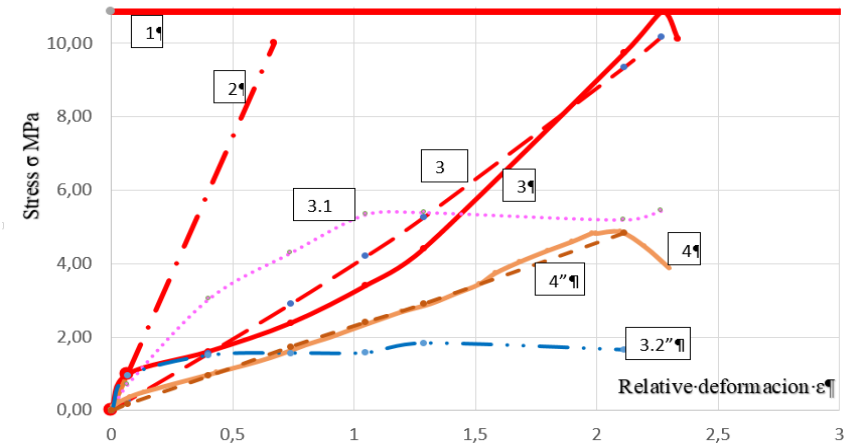

Fig. 3.15. Results of modeling the stretching of fragments of the coupling shell by various methods: 1 – ultimate strength (10.86 MPa); 2 – modulus of elasticity 14.73 MPa; 3 – experimental results – single stretching to rupture; 3" – results using the Mooney–Rivlin method for two constants; 3.1" – results using the Blatz method; 3.2" – results using the nonlinear elastic method; 4 – results of the experiment – cyclic tension to failure; 4" – results using the Mooney–Rivlin method in two constants by modifying the mesh of the model and the dimensions of the finite elements.

- **Evaluation of material modeling methods**

The Mooney–Rivlin method is more labour-intensive in modeling, but faster in SolidWorks calculations (average calculations take 15–20 min), and calculations are performed with satisfactory accuracy. The most accurate is the non-linear elastic method up to 20 mm tension, but after this value, the accuracy decreases, and the increase with this method takes about 6 times more time (more than 1.5 hours on average) than the Mooney–Rivlin method. The Blatz method shows sample thinning, and the accuracy of this type of sample turned out to be unsatisfactory (did not show accuracy for this type of task).

Next, the full rubber-cord coupling shell model can be modeled using the Mooney–Rivlin method (Fig. 3.15).

3.11. Full model modeling of rubber-cord coupling shell

The essence of the method is to divide the sector, in which the parameter we are interested in changes according to a complex law, into many sub-sectors interconnected at contact points. Due to the large deformation in the attachment area and the applied load, we remove the mesh thickening of the final elements. Considering the surface curvature of the coupling shell model, an oriented mesh was used for calculations (Fig. 3.16).

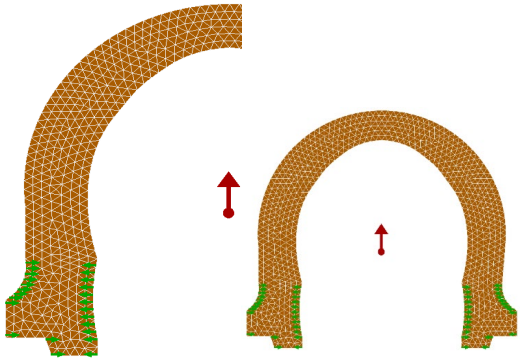

Fig. 3.16. Friction-free coupling cut.

When torque is applied to the coupling, at the point where the coupling is attached to the flanges, the coupling is elongated as a result of centrifugal force. Diagrams of the 2D model of stress and displacement along the X-axis from disk compression and rpm are shown in Figs. 3.17–3.19.

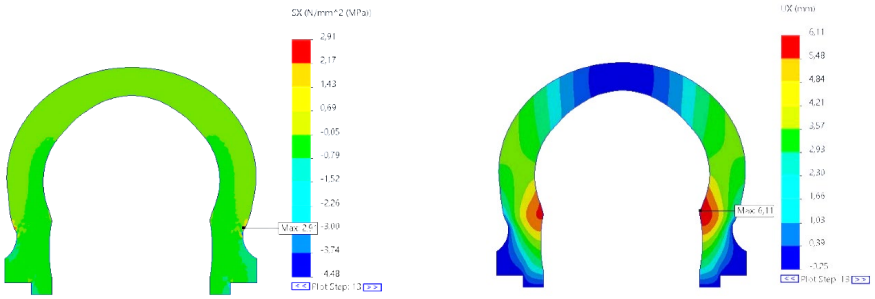

a b

Fig. 3.17. Coupling tension and extension at 64 rpm (5 km/h):
a – elemental stress along the X-axis; b – equivalent displacement along the X-axis.

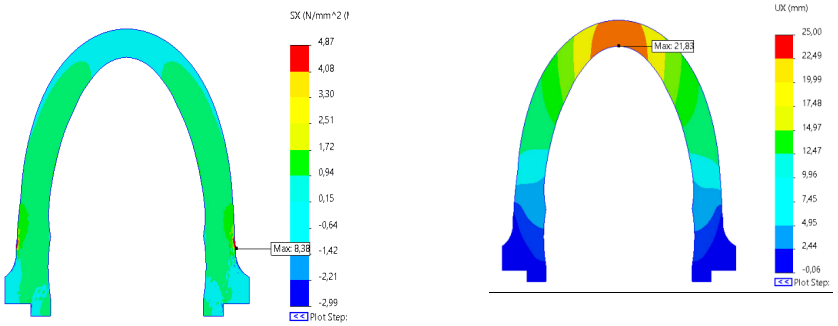

a b

Fig. 3.18. Coupling tension and extension at 1521 rpm (100 km/h):
a – elemental stress along the X-axis; b – equivalent displacement along the X-axis.

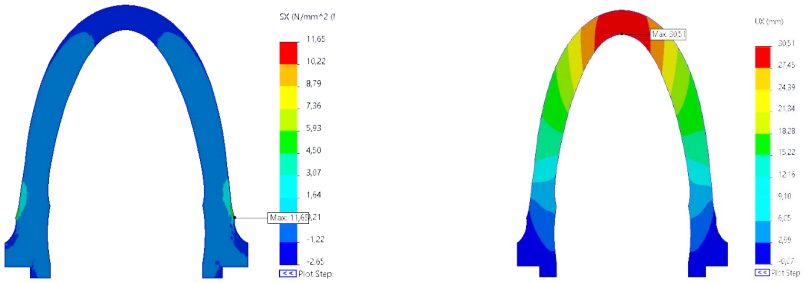

a b

Fig. 3.19. Coupling tension and extension at 1825 rpm (design speed 120 km/h):
a – elemental stress along the X-axis; b – equivalent displacement along the X-axis.

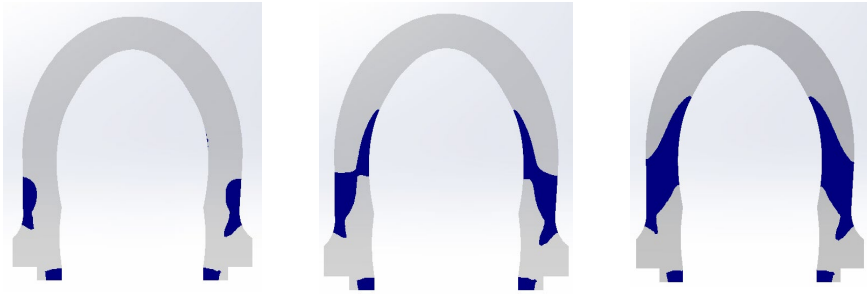

a b c

Fig. 3.20. Distribution of stresses on the surface of the coupling shell at idle:
a – 1521 rpm (100 km/h); b – 1673 rpm (110 km/h); c – 1825 rpm (120 km/h).

It was found that at a rotation speed of 1521 rpm (100 km/h) the stresses act only on the outer surface, but with an increase to 1673 rpm (110 km/h) and 1825 rpm (120 km/h) the stresses spread across the entire cross-section of the coupling.

3.12. Calculation results of radial, axial and angular deviations acting on the rubber-cord coupling

With the help of the developed calculation models, the state of the coupling stress was studied, which is affected by the following loads:

- radial;
- axial;
- angular.

Evaluating the effect of radial, axial and angular loads at a speed of 130 rpm (10 km/h), it was found that the main effect on the coupling is transferred during acceleration, since the greatest torque is exerted during this time. The effect of radial load and torque on the coupling with a maximum radial deviation of 15 mm is shown in Fig. 3.21.

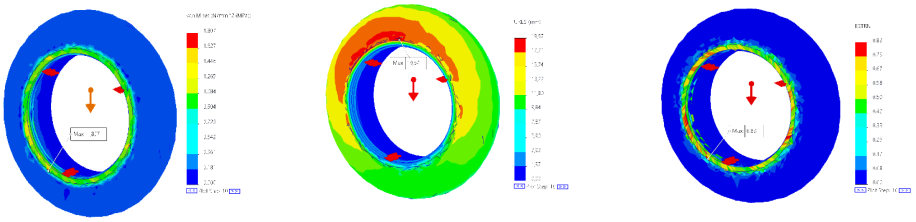

a b c

Fig. 3.21. Effect of radial load on coupling:
a – equivalent stresses; b – equivalent displacement; c – equivalent strain.

The effects of torque and radial displacement loads are unevenly distributed across the cross-section of the coupling and reach a maximum at the location of the coupling failure next to the clamping disc. The maximum stress value from the radial deviation at the coupling attachment point is 1.80 MPa, and the maximum displacement from the radial load in this case amounts to 19.67 mm.

Evaluating the influence of angular loads and torque, it was found that the main influence on the coupling is transmitted by significant deviations of the shaft inclination angles – 4 mm. The maximum stress value from the angular deviation at the attachment point of the coupling is 0.31 MPa. In this case stress are asymmetrically distributed in the walls of the clutch housing and change their sign with each revolution of the couplig. The type of coupling deformation from angular loads is shown in Fig 3.22.

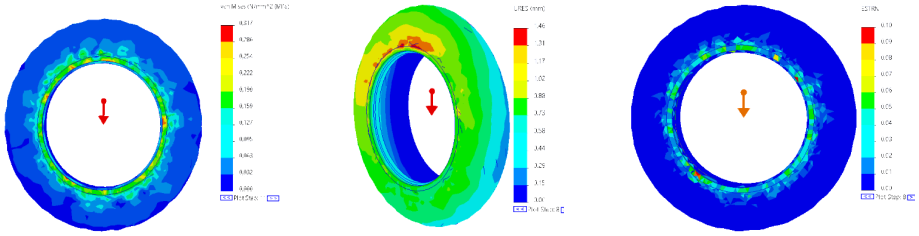

a b c

Fig. 3.22. Effect of angular load on coupling:
a – equivalent stresses; b – equivalent displacement; c – equivalent strain.

The action of the torque at a speed of 130 rpm (10 km/h) with an axial deviation of 20 mm is shown in Fig 3.23.

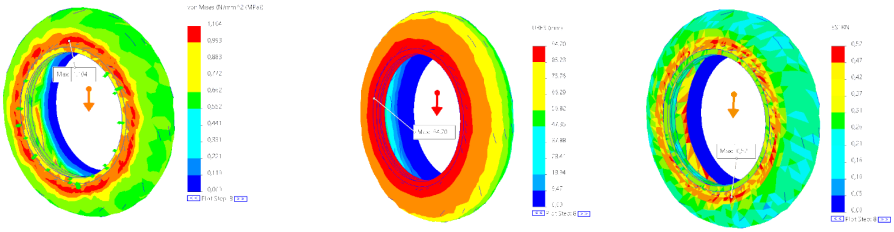

a b c

Fig. 3.23. Effect of axial load on the coupling:
a – equivalent stresses; b – equivalent displacement; c – equivalent strain.

Thus, as a result of modeling with an axial deviation of 20 mm, the maximum stress value is 1.10 MPa, and the maximum displacement (stretching) from the axial load in this case is 94.70 mm. During the radial, axial and angular deviation of the shafts, it was found that the places of damage caused by the coupling inclination angles, which appear in the simulation process, coincide with the places of damage found during operation.

3.13. Frequency analysis of rubber-cord coupling

A summary table of resonance frequencies with the largest coupling mass contribution is shown in Table 3.12.

Table 3.12

Summarized Self-frequency Results

Trial No.	Self-oscillation frequency, Hz	Coupling mass participation coefficients by axles		
		X	Y	Z
1	54.87	0.5719	1.28×10^{-6}	8.34×10^{-9}
2	56.27	0.0194	2.66×10^{-6}	3.23×10^{-6}
3	56.37	0.0260	1.97×10^{-8}	5.89×10^{-7}
11	88.25	1.82×10^{-8}	0.0533	0.3882
12	88.36	2.14×10^{-9}	0.3881	0.0532
22	126.05	4.85×10^{-7}	0.0511	0.0028
23	126.22	1.89×10^{-7}	0.0048	0.0484

These fluctuating masses represent a portion of the energy that acts on the coupling shell and can cause its damage.

As can be seen in Fig. 3.24, the first and main form of oscillation at 54.87 Hz with the largest part of the mass of the coupling 57.19 % loads the side wall of the coupling shell in the axial direction. The loaded zone coincides with the coupling failure zone during operation.

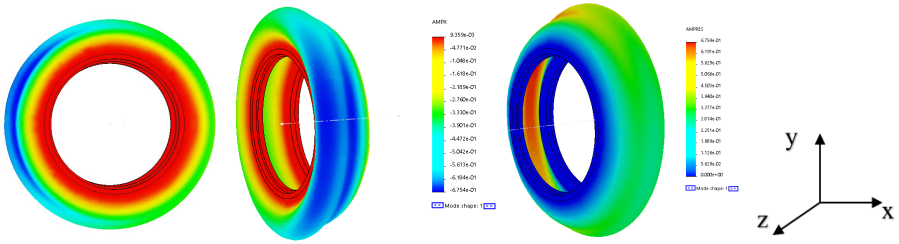

Fig. 3.24. Coupling oscillations along the X-axis with a frequency of 54.87 Hz.

As can be seen in Figs. 3.25 and 3.26.), the shape of the oscillation at the frequencies of 88.25 Hz and 88.36 Hz with the largest part of the mass of the coupling, 38.82 % and 38.81 %, respectively, directed in the radial, horizontal and vertical directions, stretches the upper surface and the side wall of the coupling shell in the radial direction. During operation, the stressed areas partially coincide with the area of coupling damage.

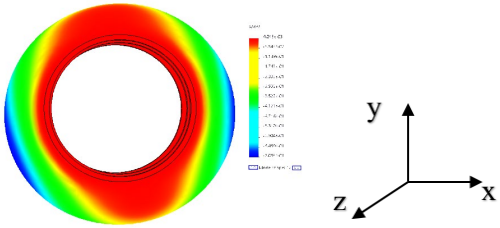

Fig. 3.25. Coupling vibrations along the Y-axis with a frequency of 88.25 Hz.

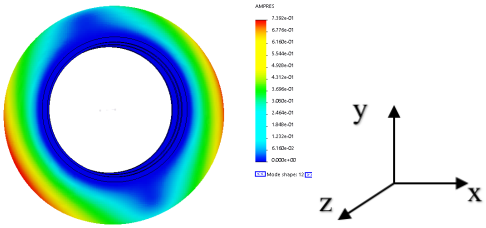

Fig. 3.26. Coupling vibrations along the Z-axis with a frequency of 88.36 Hz.

At resonance frequencies of 56.37 Hz, 56.27 Hz, 126.05 Hz, and 126.22 Hz, no more than 5 % of the mass of the rubber-cord coupling participates and its contribution does not affect the oscillations.

3.14. A review of the nature and cause of rubber-cord coupling fastening bolt fractures

The bolts used for fastening the rubber-cord coupling in rolling stock and especially in electric trains are repeatedly exposed to periodically changing loads over time and subjected to impulse, high-frequency, periodic and non-periodic, as well as variable amplitude and impact loads. As a result of exposure to repeated variable shock loads, the strength of the bolt material decreases and M24 rubber-cord coupling bolts may be prone to disintegration [13]–[17]. Examples of the breakage of M24 rubber-cord coupling bolts are shown in Fig. 3.27.

Fig. 3.27. Rubber-cord coupling degradation patterns:
a – fracture of the 1st bolt; b – two bolt fractures; c – three bolt fractures.

Under exposure to significant fluctuating and shock and impact loads, the hardening capacity of the material is exhausted, and the bolt material may be subjected to fatigue loads, resulting in periodic spalling of the top surface layer [15]–[16].

Due to many failures of M24 bolts for fastening the rubber-cord coupling, as well as the high safety requirements for fastening bolts, there is an acute question of investigating the causes of the type and nature of the bolt failure, as well as compliance of bolts with the requirements of ISO 898-1:2013 [6] and EN 10083-3:2007-01 [2] standards.

3.15. Determining the ways of disintegration of M24 bolts for the rubber-cord coupling fastening

The study of the causes of the disintegration of the M24 bolts of the rubber-cord coupling fastening according to step 10 of the metodology was carried out in the RTU laboratory according to the following directions:

- determining the type and nature of decay for three samples under static load;
- determining the type and nature of decay for three samples under cyclic loading;
- comparison of static and cyclic test data with the ISO 898-1:2013 standard;
- determining the impact viscosity at three different temperature ranges (–20 °C; 0 °C; +20 °C), and comparing the obtained data with the ISO898-1:2013 standard.

3.15.1. Determining the type and nature of decay under static loading

In order to determine the type and nature of the disintegration stress, static tests for breakage of Samples 6, 7, and 8 of M24 bolts were performed in the RTU laboratory. The bolt samples were taken from railcars with the following mileage data:

- Sample 1: mileage – 214 596 km;
- Sample 2: mileage – 105 764 km;
- Sample 3: without mileage (zero mileage).

The tests were performed in the RTU laboratory using a Zwick/Roell Z600 electromechanical testing machine with a load increase rate of 1 mm per minute.

3.15.2. Determining the type and nature of decay under cyclic loading

In order to determine the type and nature of the breakdown of M24 bolt, cyclic tests were carried out on Samples 9, 10, and 11 (stretching and unloading – 10 tests; stretching the sample to failure – 11 tests) considering three different mileage ranges:

- Sample 4: mileage – 22 543 km;
- Sample 5: mileage – 155 365 km;
- Sample 6: mileage – 210 298 km.

Cyclic tests were performed in the RTU laboratory using a Zwick/Roell Z60010 electromechanical testing machine with progressive loading and unloading. Load levels: 25 k N; 50 k N; 75 k N 100 k N; 125 k N; 150 k N; 175 k N; 200 k N; 225 k N; 250 k N. destruction. The speed of increasing the load is 7 mm per minute.

3.15.3. Determining the type and nature of decay during impact testing of M24 bolts

For this purpose, it was proposed to conduct a test on bolt Samples 7, 8, and 9 for impact resistance with similar mileage data (85 thousand km) in three different temperature ranges (–20 °C; 0 °C; +20 °C).

The data for determining the consumed energy and impact resistance data are shown in Table 3.13.

Table 3.13

Determining the Sample Parameters at Different Temperatures

Sample parameters	Sample No.		
	12	13	14
Test temperature t, °C	+20	0	–20
Potential energy A, J	450	450	450
* Absorbed energy A_1, J	54.3	39.1	21.7
Conditional impact resistance a_k, J/mm^2	67.9	48.7	26.9

* According to ISO 898-1:2013 requirements absorbed energy – min 27J, for full profile test sample.

3.16. Examining M24 bolts for compliance with ISO 898-1:2013 EN 10083-3:2007-01

To determine the causes of bolt disintegration, check the compliance of the samples with the requirements of ISO 898-1:2013 [2] and EN 10083-3:2007-01 [2] standards for 4Cr41 grade steel. Broken bolt Samples 10, 11, ; No,12; No.13 which were dismantled from ER2 and ER2T series motor cars were chosen as research objects;, as well as one sample No.14. of a new bolt. The research was carried out in the laboratory of the Riga Technical University in the following directions:

- determination of hardness;
- chemical composition analysis;

The obtained data have been approved by the independent laboratory "KIWA" Inspecta.

The data on the mileage and the operating time of the bolts in the cars are shown in (Table 3.13.).

Table 3.13

Data on the Performance of Bolts

Sample No.	Car No.	TR-3 repair completion date	Date of arrival	Operating time, days	Mileage, km
1	1342-02	12.12.2019	29.06.2020	201	59 348
2	3034-06	23.05.2020	30.10.2020	160	64 078
3	7117-04	20.11.2020	02.01.2021	43	17 124
4	7113-06	20.04.2020	03.06.2021	408	114 400
5	new bolt	-	-	-	-

- **Determining the hardness**

In the laboratory of Riga Technical University, steel hardness was tested according to the Brinell scale (HB) [18] using the MIC 10 device [11]. In order to obtain greater accuracy of the experiment, measurements were made at 5 points along the entire cross-section of the samples.

The dependence of the hardness HB on the mileage of the bolts is shown in Fig. 3.28.

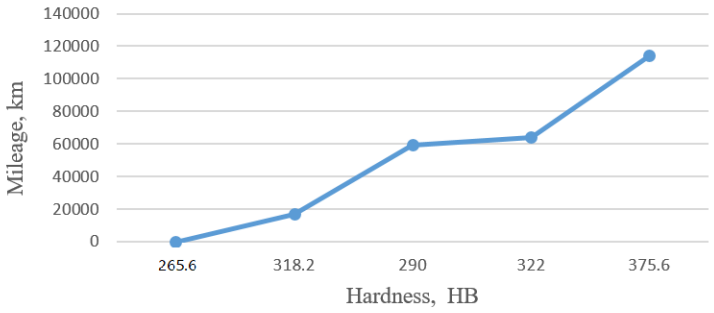

Fig. 3.28. Dependence of hardness of the coupling bolts on mileage.

According to the results in the graph, we can see that the hardness of the coupling bolts increases with increasing mileage, i.e. the material of the bolts becomes stronger.

- **Chemical composition analysis**

According to the analysis results of chemical composition of steel, it was found that:

- steel grade of Sample 10 – not determined;
- steel grade of Sample 11 – 34Cr4;
- steel grade of Sample 12 – not determined;
- steel grade of Sample 13 – not determined;
- steel grade of Sample 14 – 34Cr4.

During the investigation of the chemical composition of the steel, the following inconsistencies with the requirements of standard EN 10083-3:2007-01[2] were discovered.

The carbon (C) content in four samples is less than the norm and amounts to:

- in Sample 2 – 0.366 %;
- in Sample 3 – 0.261 %;
- in Sample 4 – 0.316 %;
- in Sample 5 – 0.322 %;
- however, in Sample 1, the carbon content exceeds the norm and is 0.505 %.

On the other hand, according to the requirements of the EN 10083-3:2007-01 [2] standard, the carbon content of the steel grade 4Cr41 should be within 0.38–0.45 %. As the amount of carbon in the steel decreases, its plasticity improves and rigidity (impact resistance) increases. As the carbon content in the steel increases, the hardness, strength and rigidity of the steel increases, the yield strength σ_t and tensile strength σ_s also increase, but at the same time plasticity and impact resistance decrease, and machinability and weldability also deteriorate [23]–[24].

Harmful impurities of phosphorus and sulphur were found in the material of the bolts during the research process. The percentage of phosphorus (*P*) in Sample 1 was 0.125 %, in Sample 2 – 0.0050 %, in Sample 3 – 0.0813 %, in Sample 4 – 0.0898 %, and in Sample 5 – 0.0671 %. In four samples, the phosphorus content significantly exceeds the norms set by the EN 10083-3:2007-01 [2] standard, which should be less than 0.025 %.

3.17. Metallographic analysis of the bolt samples

To confirm the presence of defects in the microstructure, Samples 10 and 11 were subjected to metallographic analysis. Based on the results of the research, the presence of impurities and cracks was found in the metallographic structure of the bolts. The metallographic structure of M24 bolts is shown in Figs. 3.29 and 3.30.

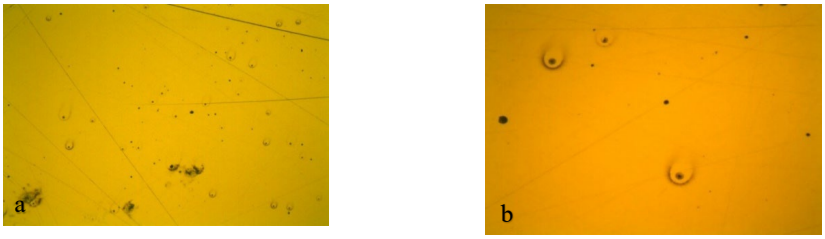

Fig. 3.29. Microstructure of bolt Sample 10, magnification: a – × 50; b – × 200.

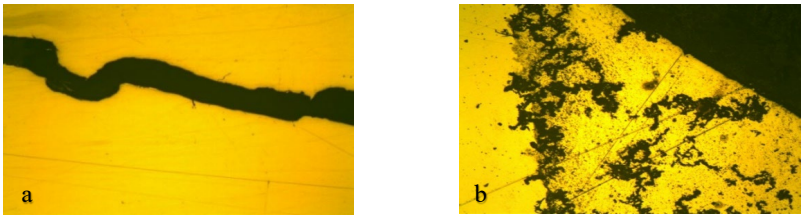

Fig. 3.30. Microstructure of bolt Sample 11, magnification: a – × 50; b – × 200.

Metallographic analysis revealed a large number of non-metallic impurities in all samples. As the bolt's life (mileage) increases, the impurities increase in number and size, later causing fractures.

In Latvian railways, the rubber-cord coupling fastening bolts were subjected to shock loads under operating conditions. When studying the microstructure of the bolts, it was found that there is a gradual accumulation of defects resulting from the action of the impact load. In order to control the magnitude of the impact load, a device has been developed that records the magnitude of the impact load in operation.

3.18. Design of impact and vibration force control devices for bolted fasteners

The purpose of the invention is to create a device for controlling the impact and vibration force of bolt fastenings, which would make it possible to constantly accumulate and analyze data on the impact force received by the bolts during the operation of the vehicle in order to reduce the number of unplanned repairs of rolling stock of railway transport or vehicles of other industries due to its damage, as well as to reduce the number of accidents [14]. The block diagram of the invented devices is shown in Fig. 3.31.

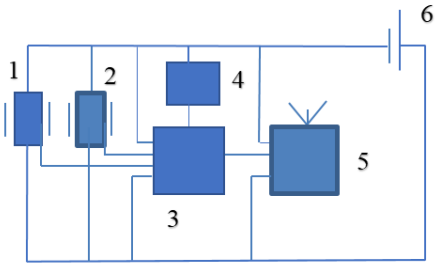

Fig. 3.31. Block diagram of the invented device:
1 – vibration sensor; 2 shock sensor; 3 – microcontroller; 4 memory module; 5 data transmission unit; 6 – power supply unit.

The purpose of the invention is achieved as follows: the device for controlling the impact and vibration force of bolt fasteners consists of a housing, inside which the following elements are installed: a vibration sensor (4) and an impact sensor (5), a microcontroller (6), a data transmission unit (7) and a power supply unit (8). A piezo-accelerometer can be used as a vibration sensor (4) and shock sensor (5) – sensors that convert the value of vibration or shock force into an electronic signal [12]–[9].

Putting the invented device into operation will allow obtaining objective data on the impact force and vibration loads on the bolts. Accumulating information and processing it regularly can prevent damage to rubber-cord coupling bolts and, accordingly, reduce the number of unplanned repairs of electric trains. The invention can be used in any type of railway rolling stock, as well as metro cars. The invented device can be used in mechanical engineering, shipbuilding and other industries to control the defect of sleepers, deviations of shafts, the condition of gear transmissions and other structures on which the fixing bolts are subjected to deformation forces. If during processing the information received from the device of the invention during technical maintenance (or restoration repair) it is found that the allowable loads have been exceeded many times, then the bolts must be replaced with new ones. Thus, the need to perform unplanned repairs due to bolt damage, which are associated with large financial costs for the company, is avoided [3]–[4].

3.19. Testing of the shock vibration device

In order to do this, it was necessary to determine the impact force F, which is received by the bolts when the moror car crosses the rail joints. The impact force F, which is absorbed by the bolts of the rubber-cord coupling, is determined according to Formula (3.4). To determine it, it is necessary to determine the acceleration with which the motor car crosses the rail joint. For this purpose, we use the empirical Formula (3.5).

$$F = \omega_r \cdot q, \tag{3.4}$$

where q is half the mass of the wheelset, t, and ω_r is the acceleration with which a car crosses a rail joint, m/s^2.

$$\omega_r = \left[2 + 0.13\frac{V}{\sqrt[3]{(2q)^2}}\right] \cdot g, \tag{3.5}$$

where V is the car speed, km/h; q is half the mass of the wheelset, kg; and g is acceleration of free fall, 9.81 m/s^2.

The data of acceleration and impact force calculations are presented in Table 3.15.

Table 3.15

Acceleration and Impact Load Calculation Data

Car speed V, km/h	Acceleration of the wheelset ω_r, m/s^2	Impact power F, N
20	28.122	42 183
40	36.624	54 936
60	45.126	67 689
80	53.628	80 442
100	62.13	93 195
120	70.632	105 948

Next, in order to determine the impact load, crushing load tests of rubber-cord coupling fastening bolts were conducted at the State Joint Stock Company "Latvijas dzelzceļš" that operates the electric train, using the developed impact vibration device, with different, close to the calculated impact force F data. The trial data is shown in Table 3.16.

Table 3.16

Testing the Impact Vibration Device on the Bench

Trial No.	Quantity of bolts, pcs	The impact force F, N	Quantity of blows, pcs.	Impact level size, cond. units.
1	16	20 000	1000	305–317
2	16	40 000	730	329–338
3	16	60 000	467	354–362
4	16	80 000	354	383–395
5	16	100 000	136	418–430

Analyzing bolt impact test data, it was found that with an impact force equal to:

- 20 000 N (2 tons) – bolts do not break;
- 40 000 N (4 tons) – after the 730th impact, one bolt broke;
- 60 000 N (6 tons) – after the 467th impact, one bolt disintegrated, but after 500 hits the second bolt was found to have disintegrated during the inspection of the bolts;

- 80 000 N (8 tons) – after the 354th impact, one bolt disintegrated, but after 360 impacts, the disintegration of the second bolt was found during the inspection of the bolts;
- 100 000 N (10 tons) – after the 136th impact, it was found that two bolts were subject to disintegration at once, after testing of 150 impacts, it was found that disintegration took place in two more bolts, which are critical in operation.

Metallographic analysis of bolts subjected to impact loads of 20 000 N and 100 000 N is shown in Figs. 3.32 and 3.33.

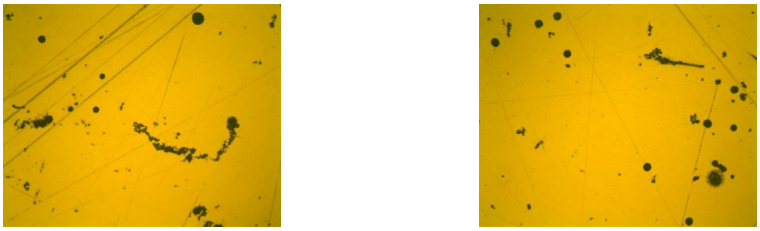

a b

Fig. 3.32. Metallographic analysis after 360 impacts with a force of 20 000 N, magnification – × 200:
a – Sample 15; b – Sample 16.

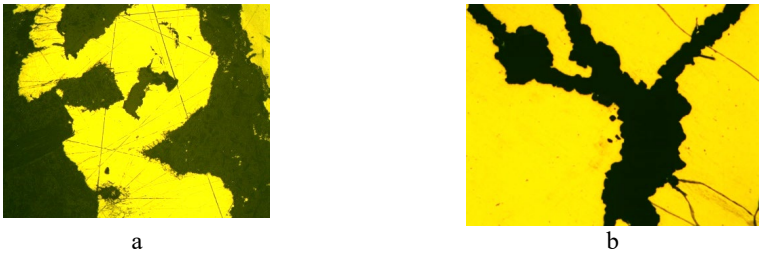

a b

Fig. 3.33. Metallographic analysis after 360 impacts with a force of 100 000 N, magnification – × 200:
a – Sample 17; b – Sample 18.

Metallographic analysis confirmed the formation of critical defects and cracks in the microstructure at different values of the impact load, which caused the bolt to disintegrate.

To check the shock vibration load received by the rubber-cord coupling bolts, a shock vibration device was installed on the rubber-cord coupling flange. The installation location of the device is shown in Fig. 3.34. The operation test of the shock vibration device was performed on electric train motor car No.7118 10 starting from 15.03.2023. The results obtained from the impact vibration device are shown in Fig. 3.35.

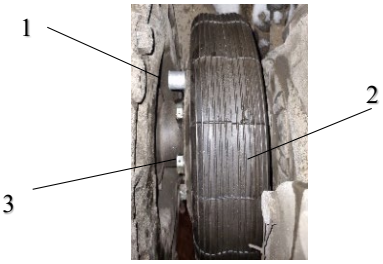

Fig. 3.34. Placement of shock vibration device:
1 – impact vibration device; 2 – rubber cord coupling; 3 – fastening bolt.

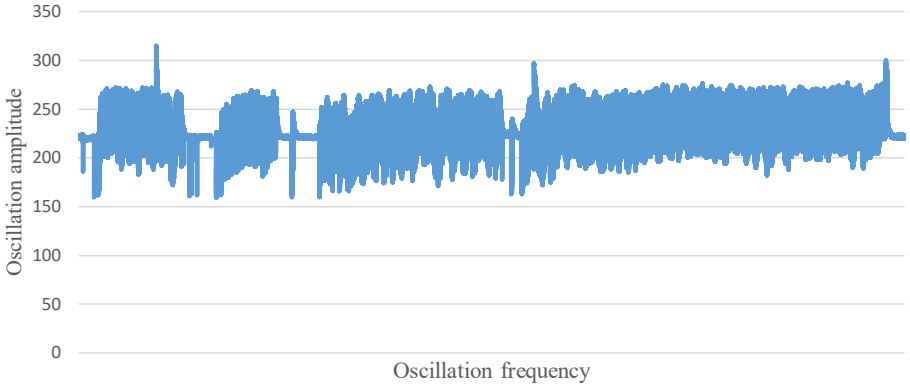

Fig. 3.35. Shock vibration load graph for one working day.

Figure 3.35 shows the shock vibration load level of car No.7118-10 for a working day. The determined amount of hits of more than 300 cond. units consists of 3 cases. The mileage of the car is 486 km.

Once a month, when the motor car reached 10–15 thousand km mileage, one bolt was dismantled for metallographic analysis. The data of the study of the performance of bolts using an impact vibration device are shown in Table. 3.17.

Table 3.17

Impact Load Determining

Sample No.	M24 bolt performance indicators				
	Mileage, km	Readings of the vibration force control device, cond. units			
		300–330	331–360	361–390	391–420
21	12 682	52	14	3	0
22	25 632	116	21	4	2
23	38 850	187	33	5	3
24	52 512	236	42	8	3
25	65 748	287	50	12	4
26	79 906	314	61	15	5
Critical level	264 000	700	250	150	40

During the monitoring, the maximum impact vibration level of the impact load was 396 conditional units.
The results of metallographic analysis of bolt Samples 21 and 26 are shown in Figs. 3.36 and 3.37, magnification – × 100.

Fig. 3.36. Metallographic analysis of bolt Sample 21, mileage 12 882 km.

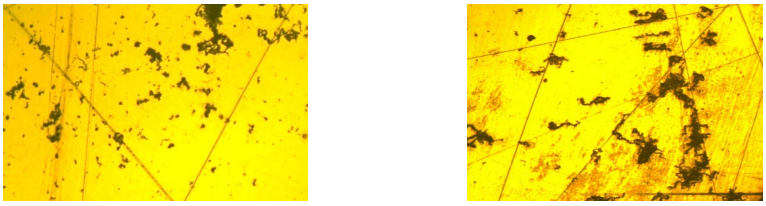

Fig. 3.37. Metallographic analysis of bolt Sample 26, mileage 79 906 km.

The results of the metallographic analysis showed the gradual formation of defects in the microstructure.

3.20. The economic effect of the implementation of the methodology and the introduction of impact vibration devices into operation

The implementation of the methodology into operation will give the following results – there will be no costs for unplanned repairs, but the human factor must be taken into account. The costs will be related only to the implementation of the impact vibration device and methodology into operation. Data on unplanned repair costs are given in Table 3.18 [13].

Table 3.18

The Costs of Unplanned Repairs

The name of the unplanned repair	1st unplanned repair, EUR	Unplanned repairs for 10 years, EUR	Introduction of impact vibration devices into operation, EUR
Replacing the rubber-cord coupling bolts	429	103 895	15 000
Replacing the rubber-cord coupling	575	58 842	

According to the result data (Table 3.18), the costs for the installation of the impact vibration device and the implementation of the methodology will pay off within 2 years.

CONCLUSIONS

Summarizing the work results and based on them, the following conclusions can be drawn.

1. Statistical data on the failures of rubber-cord couplings and their fastening bolts during the period from 2012 to 2021 was studied in detail. The number of failures of rubber cord couplings was 101, and the number of failures of their fastening bolts – 298. Also, in the Doctoral Thesis, an evaluation of the failures of couplings and bolts by season was carried out, and it was found that the largest number of failures is attributable to the winter period:
   • the number of failures of rubber-cord couplings is more than 41 %,
   • the number of failures of rubber-cord coupling fastening bolts is more than 43 %.
2. During the research of the rubber-cord coupling and their fastening bolts, in accordance with the developed methodology and during their approval, the following results were obtained:
   • After a visual inspection, it was found that 95 % of the damage to the rubber-cord couplings is the destruction of the side surfaces, which are located 10–20 mm away from the place where the coupling is attached to the flanges.
   • After measuring the temperature of the rubber cord couplings in the conditions of Latvian railways, it was found that the condition for the coupling not to heat up more than +75 ºC is observed in 100 % of cases, in accordance with the requirements of standard ISO 14691:2008.
   • According to the results of measuring the geometric dimensions of rubber-cord couplings, it was found that the outer diameter *D* of 6 % rubber-cord couplings does not meet the requirements of the ISO 14691:2008 standard; therefore it was proposed to replace the rubber-cord couplings with non-compliant outer diameter with new ones.

- According to measurements of the hardness of rubber-cord couplings, it has been experimentally proven that at temperature ranges:
  - –20 °C to 0 °C – 88 % of couplings do not meet the requirements of standard ISO 14691:2008, exceeding the standard data by 11.4–4.2 conditional units;
  - +5 °C to +10 °C – 52 % of couplings do not meet the requirements of standard ISO 14691:2008, exceeding the standard data by 9.2 conditional units;
  - +15 °C to +20 °C – 20% of couplings are non-compliant with the requirements of standard ISO 14691:2008, exceeding the standard data by 4.8 conditional units.

According to the hardness measurement results, it is recommended to replace one of the four rubber-cord coupling due to non-compliance with ISO 14691:2008 standard requirements at different temperature ranges.

Concerning the other non-compliances of rubber-cord couplings with the requirements of the ISO 14691:2008 standard, a recommendation is made to the manufacturer.

- Based on the experiments carried out in the Thesis, it was proved that the failures of the rubber-cord coupling fastening bolts are related to the crushing processes from metal fatigue due to accumulation of defects in the microstructure, which is also confirmed by the metallographic analysis of the crushing diagrams of new bolts without defects in the microstructure and bolts with mileage and the presence of defects in the microstructure.
- According to the results of microstructure studies using metallographic analysis, the amount of microstructure defect formation in bolts was found, which increases with the increase of bolt operation time (mileage).
  - The reliability and accuracy of the obtained bolt results are confirmed in the certified testing laboratory KIWA JSC "Inspecta Latvia".

3. After creating the calculation model in the SolidWorks program, using selected Mooney–Rivlin elastomeric material models, the following results were obtained:

- By modeling the maximum axial, radial and angular deflection data, it was found that the total stress action from axial, radial and angular deflections under cyclic loading is dangerous for couplings and can cause lateral surface disintegration, as it reaches 3.21 MPa, which is more than 60 % of the strength limit σ_b (4.87 MPa), which causes disintegration of the side surface under cyclic loading.
- When modeling different ranges of angular velocities, it was found that at 1670 rpm, which corresponds to more than 110 km/h, the stress at the coupling attachment place of to the flanges more than 2 times exceeds the strength limit σ_b under cyclic loading and begins to spread throughout the coupling cross section.
- While studying the influence of the first 40 resonance frequencies in the SolidWorks finite element modeling program, the tension zones of the rubber-cord coupling were determined, and it was found that due to the critical frequencies of resonance the X-, Y-, and Z-axes experience coupling oscillations involving a certain amount of coupling mass. The most dangerous resonance frequencies are along the X-axis, when more than 57 % of the coupling mass participates in the oscillations. At this frequency, the coupling zones are subject to deformation, and they coincide with the damage zones

that are detected in operation. To reduce the risk of damage to the coupling shell, it is necessary to prevent long-term operation of the coupling at the calculated critical frequencies – 54.87 Hz, 88.25 Hz, and 88.36 Hz.

- Modeling results in the SolidWorks program confirmed that at high torque and axial, radial or angular deviation, as well as at high rotation frequency, the most stressed area of the coupling is its side surface near the outer diameter disc attachment point.

4. In order to reduce the number of bolt failures, a shock vibration load monitoring device was developed, which was tested on rolling stock, and using this device shock vibration load level data were obtained in real operating conditions.
   - By studying the data obtained by the impact vibration device, the critical value of the impact load was determined, at which it was recommended to replace the fastening bolts of the rubber-cord coupling. The results were also confirmed by metallographic analysis when microcracks and a large number of microstructure defects were detected.

LIST OF REFERENCES

1. DIN EN 13913:2003-08 railway applications – rubber suspension components – elastomer-based mechanical parts, 54 p.
2. EN 10083-3:2007-01 Technical delivery conditions for alloy steels. English version. p. 54.
3. Gavrilovs, P., Dmitrijevs, A. Research in passenger car bogie central suspension roller and rod base metal and welded metal structure. Engineering for Rural Development, 2016, pp. 618–623.
4. Gavrilovs, P., Ivanovs, V. Research of the defective frog wing of 1/11 mark Transport Problems, 2017, 12 (4), pp. 119–126.
5. Gorbacovs, D., Mihailovs, F., Eiduks, J. Analysis of the Formation of Defects in the Microstructure of the M-24 Bolts of the Rubber-Cord Coupling at Various Ranges of Mileage of Electric Trains Motor Cars, 2021, pp. 1–4, IEEE.
6. ISO 898-1:2013 Mechanical properties of fasteners made of carbon steel and alloy steel, 27 p.
7. ISO 7619-1:2010 Rubber, vulcanized or thermoplastic – Determination of indentation hardness – Part 1: Durometer method (Shore hardness), 10 p.
8. ISO 14691:2008 Petroleum, petrochemical and natural gas flexible couplings for mechanical power transmission. General-purpose applications, 32 p.
9. Komorska, I., Vibroacoustic Diagnostic Model of the Vehicle Drive System, 2011, 130 p., ISBN-10: 837789016X, ISBN-13: 978-8377890165.
10. Kucherskij, A. M. A promising method for measuring hardness of rubber / A. M. Kucherskij // Polymer Testing. 1997, No. 16, pp. 481–490.
11. Kuzu, C., Pelit, E., Meral, İ. A new design of Rockwell-Brinell-Vickers hardness standard machine at UME, Acta IMEKO, 2021, 9 (5), pp. 230–234.

12. Leonardson, R., MacGugan, D. Design and fabrication of a commercial triaxial accelerometer, Sensors (Peterborough, NH), 1994, 11 (8), pp. 22–23.
13. Mihailovs, F., Eiduks, J., Gorbačovs, D. Reducing the number of unscheduled repairs of traction gear of EMU trains by introducing modern technical solutions. 10th International Scientific Conference "Rual Development", 2021, Kaunas, Lithuania, vol. 6.
14. Stauffer, J.-M. Market opportunities for advanced MEMS accelerometers and overview of actual capabilities vs. required specifications. Record – IEEE PLANS, Position Location and Navigation Symposium, 2004, pp. 78–82.
15. Steels Microstructure and Properties, Fourth edition, Harshad Bhadeshia, Robert Honeycombe, 2017, eBook ISBN: 978-0-08-100272-8, Hardcover ISBN: 978-0-08-100270-4, p. 488.
16. Taylor, J., Mehmanparast, A., Kulka, R., Moore, P., Farrahi, G. H., Xu, L. Compact crack arrest testing and analysis of EH47 shipbuilding steel, Theoretical and Applied Fracture Mechanics, 2021, art. no. 103004.
17. Zaripov, R., Gavrilovs, P, Sembaev, N. Study of the stressed-deformed condition of a railway tank car with shock loading taking into account the decrease of fastenings, Transport Means – Proceedings of the International Conference, 2019, pp. 1112–1116.
18. Zhang, Z.-J., Zheng, P.-F., Chen, H., Cai, L.-X. The method for hardness prediction of metal materials based on energy equivalence principle, Gongcheng Lixue/Engineering Mechanics, 2021, 38 (3), pp. 17–26.
19. Elektrovilcienu tekošā remontu un tehniskas apkalpošanas noteikumi L31/97, Valsts akciju sabiedrība "Latvijas dzelzceļš", Rīga, 1997g. 152 lpp.
20. AS "Pasažieru vilciens" vilces ritošā sastāva tehnisko apkopju un remontu sistēma Rīkojums Nr. 38-2021, 2021, 5 lpp.
21. Бирюков, И. В., Беляев, А. И., Рыбников, Е. К. Тяговые передачи электроподвижного состава железных дорог. – М.: Транспорт, 1986. 256 с.
22. Задель, Х. Э., Коген-Далин, В. В., Крымов, В. В., Электротехника Москва: Высшая школа, 1985. 480 стр.
23. Никифоров, В. М. Технология металлов и других конструкционных материалов: Москва: 2015. 384 стр.
24. Сучков, О. К., Пятигорский, М. Г., Технология металов и конструкционные материалы Москва: 1974. 446 стр.
25. Спиридонова, М. П. Эластомерные материалы, содержащие молекулярные комплексы и комплексные соединения с ε-капролактамом Волгоград, 2019, 352 стр.
26. Тагер, А. А. Физикохимия полимеров Москва: Химия 1978. 544 стр.
27. Тимофеев, С. И. Детали машин – Ростов, Феникс, 2005, 409 стр. ISBN 5-222-05122-6 (в пер).
28. Эмануэль, Н. М., Бучаченко, А. Л. Химическая физика старения полимеров. Москва: Наука, 1984. 342 стр.

Dmitrijs Gorbačovs was born in 1974 in Riga. He obtained a Bachelor's degree (2008) and a Master's degree (2012) from Riga Technical University. He was a locksmith at the Riga Locomotive Depot (1994–2001) and at JSC "LDz Ritošā sastāva serviss" (2001–2007). Since 2007, he has been a senior engineer-technologist of JSC "Pasažieru vilciens". He received various awards from the Latvian Railway Transport Company, including the Award for Long-term Work in the Railway Industry (2009), the Award of the Best JSC LDz Engineer (2012), and the Certificate of Appreciation for Developing Professional Skills and Training New Employees (2012).
His scientific interests are related to research in the railway transport sector.